9.1 Introduction

In this chapter instruments and dosimeters currently used in the environment of particle accelerators to measure and characterize the radiation fields is discussed. The emphasis here is on instrumentation that addresses those aspects of accelerator radiation fields that pose special problems that are somewhat unique to this branch of radiation protection. Thomas and Stevenson (Th88) and Swanson and Thomas (Sw90) also discuss these matters. Cember (Ce69) has also described the basics of radiation measurement instrumentation quite well. Knoll (Kn79) has also written an excellent treatise on this subject. Virtually all particle detection techniques that have been devised by physicists have, to some degree, been employed in radiation measurements at accelerators. For example, the particle yields discussed previously are to a large degree a product of the basic scientific research program for which the accelerators have been built. The radiation protection practitioner needs to be able to astutely determine which data, among the flood of results which pours out of the physics experiments, can be applied to problems of practical interest in radiation protection.

9.2 Counting Statistics

Many of the detection techniques employed to measure radiation fields are directly, or indirectly, dependent upon the counting of individual events such as the passage of charged particles through some medium or the decay of some particle, or radionuclide. Cember (Ce69) has given a good summary of **counting statistics** that bears repeating here. Radioactive decays are randomly occurring events having a sampling distribution that is correctly described by the **binomial distribution** given by the expansion of the following:

$$(p+q)^n = p^n + np^{n-1}q + \frac{n(n-1)}{2!}p^{n-2}q^2 + \frac{n(n-1)(n-2)}{3!}p^{n-3}q^3 + \ldots, \qquad (9.1)$$

where p is the mean probability for occurrence of an event, q is the mean probability of non-occurrence of the event so that $p + q = 1$, and n is the number of chances of occurrence. The probability of exactly n events occurring is given by the first term, the probability of (n - *1*) events is given by the second term, etc. For example, in the throwing of a dice, the probability of throwing a "one" is 1/6 and the probability of throwing a "one" 3 times in a row (n = 3) is:

$$p^n = (1/6)^3 = 1/216. \qquad (9.2)$$

In three throws, the probabilities of throwing 2 "ones", 1 "one" and no "ones" are given by the 2nd, 3rd, and 4th terms of the expansion; 15/216, 75/216, and 125/216, respectively.

This distribution becomes essentially equivalent to the **normal or Gaussian distribution** when *n* has an approximate value of at least 30. The Gaussian distribution is as follows:

$$p(n) = \frac{1}{\sigma\sqrt{2\pi}} \exp\left[-(n-\bar{n})^2 / (2\sigma^2)\right] , \tag{9.3}$$

where $p(n)$ is the probability of finding exactly n, $\bar{n}$ is the mean value, and σ is the standard deviation.

Radioactive decays or particle reactions can often be characterized as highly improbable events. For such "rare" events, the binomial distribution approaches the **Poisson distribution**. In this distribution, the probability of obtaining *n* events if the mean value is $\bar{n}$ **,** is given by:

$$p(n) = \frac{(\bar{n})^n e^{-\bar{n}}}{n!} . \tag{9.4}$$

For example consider 10^{-3} μCi of activity. For this, $\bar{n}$ = 37 decays sec^{-1}. The probability of exactly observing this number of events in any one second is

$$p(37) = \frac{(37)^{37} e^{-37}}{37!} , \tag{9.5}$$

where one can apply Sterling's approximation,

$$n! = \sqrt{2\pi n}\left(\frac{n}{e}\right)^n , \tag{9.6}$$

to evaluate the factorial. Thus p (37) = 0.066. As in the case of the normal distribution, 68 % of the events would lie within one standard deviation of the mean, 96 % of the events would lie within 2 standard deviations of the mean, etc. For the Poisson distribution, the standard deviation is given by

$$\sigma = \sqrt{n} . \tag{9.7}$$

The relative error, σ/n, is thus $\sqrt{n}/n$.

Often, when dealing with instrumentation, counting rates are involved. For these the following holds:

$$r \pm \sigma_r = \frac{n}{t} \pm \frac{\sqrt{n}}{t} , \tag{9.8}$$

where r is the counting rate per unit time, σ_r is its standard deviation, and t is the counting time during which the rate is measured. The quantity t, for example, could even be the integration time constant of some instrument. It follows that,

$$\sigma_r = \frac{\sqrt{n}}{t} = \sqrt{\frac{n}{t}\cdot\frac{1}{t}} = \sqrt{\frac{r}{t}}\,. \tag{9.9}$$

Usually, counts due to background radiations are present and must be dealt with. The standard deviation of the **net counting rate** is

$$\sigma_n = \sqrt{\sigma_g^2 + \sigma_{bg}^2} = \sqrt{\frac{r_g}{t_g} + \frac{r_{bg}}{t_{bg}}}\ , \tag{9.10}$$

where the subscripts g refer to the measurement of the *gross* counting rate while the subscripts bg refer to the measurement of the *background* counting rate. In general, the common statistical tests are valid for Poisson statistics.

Another quantity that sometimes becomes important is the resolving time of an instrument. This is the time that the detector, following an event, is incapable of measuring a second event. It can be measured by exposure to two different sources of radiation. In such a measurement, certain detector has a measured background rate of R_{bg} and responds to first source alone with a rate R_1 and to the second source alone with a rate R_2 where both R_1 and R_2 include the background. When exposed to the two sources simultaneously, the measured rate is R_{12}. The **resolving time**, τ, is given by (Ce69);

$$\tau = \frac{R_1 + R_2 - R_{12} - R_{bg}}{R_{12}^2 - R_1^2 - R_2^2}\,. \tag{9.11}$$

In many situations, it is often easier to determine τ from the physical properties of the detection mechanism or from the electronic time constants related to the resolving time in the measurement circuitry. When the observed counting rate of a sample is R_o, then the "true" counting rate, R, that would have been observed with a *perfect* instrument having a resolving time of zero is given by

$$R = \frac{R_0}{1 - R_0\tau}\,. \tag{9.12}$$

Knoll (Kn79) has provided a very detailed discussion of count rate considerations and the optimization of the counting statistics.

9.3 Special Considerations for Accelerator Environments

There are a number of features of accelerator radiation fields which merit attention in choosing instrumentation or measurement techniques. The most important of these are discussed here.

9.3.1 Large Range of Flux Densities, Absorbed Dose Rates, etc.

The magnitudes of the quantities to be measured encountered at accelerators may range from fractional mrem yr^{-1} needed for environmental monitoring and studies to the very large values of absorbed dose, up to megarads (10^6 rads) or so, of concern in radiation damage situations. It is customary to quantify radiation fields in terms of absorbed dose at levels above those encountered in personnel protection ($\approx$ 1 rad).

9.3.2 Possible Large Instantaneous Values of Flux Densities, Absorbed Dose Rates, etc.

Certain accelerators such as linacs, rapid cycle synchrotrons, and "single-turn" extracted beams from synchrotrons can have very low average flux densities, etc. but have extremely high instantaneous rates. Such circumstances arise at accelerators at high intensities or in situations where the **duty factor**, the fraction of the time the beam is actually present because of accelerator characteristics, of a high intensity radiation field is small. Thus, the dead time considerations described above must be taken into account or the measured results can be found to be misleadingly low. Some instruments can be completely paralyzed by high instantaneous rates. Thus, the effect of dead-time on the instantaneous counting rate that is present needs careful consideration.

9.3.3 Large Dynamic Range of Neutron Radiation Fields

At any given accelerator capable of producing neutrons, the properties of nuclear interactions make it highly probable that neutrons will be present at all energies from thermal ($<E_n> \approx 0.025$ eV) up to the energy of the beam. As will be discussed shortly, the methods of detection of neutrons vary considerably over this energy domain. Thus the choice of instrumentation is crucial to the success of the measurement. For no other particle-type is the energy range of the particles encountered in the accelerator environment so large. For no other particles are the types of effective detection techniques so diverse.

9.3.4 Presence of Mixed Radiation Fields

At accelerators, one has to consider that any given radiation field external to shielding is likely to be comprised of a mixture of photons, neutrons, and at high energies and at forward angles, muons and even a multitude of other particles. Interior to shielding, the

multiplicity of particle types present can be quite large. Also, virtually all neutron fields contain at least some photon component due, at least, to the capture of thermal neutrons by means of (n, γ) reactions. Also, muon fields near proton and ion accelerators commonly contain some neutron component. Thus the choice of instrumentation is somewhat dependent upon what particles are present in addition to the one being measured. In certain situations, the radiation field component that is not of interest can actually mask the one of concern.

9.3.5 Directional Sensitivity

Certain instruments intrinsically exhibit directional sensitivity. This feature can be either beneficial or detrimental, depending upon the situation. In all instances, it must be understood. It can lead to underestimates in radiation fields where all particles are not mono-directional. Directional sensitivity can actually be useful in certain circumstances to identify sources of unwanted radiation.

9.3.6 Sensitivity to Features of the Accelerator Environment Other than Ionizing Radiation

While the focus of this discussion is on ionizing radiation, other features must be taken into account. The most prominent of these is the presence of radio-frequency radiation (RF) at some locations that can perturb instruments, which can act, sometimes rather effectively, as "antennas". Environmental effects such as temperature and humidity can also be important. In addition, one must use caution when attempting radiation measurements in the presence of magnetic fields. Induced Eddy currents might be interpreted as radiation-induced ionization. Instruments may become magnetized and meter movements may be damaged.

9.4 Standard Instruments and Dosimeters

This section will review instruments and dosimeters. Some of these are commonly available from commercial sources. However, commercial instruments should be used with care at accelerator facilities to be sure that their properties are adequate for usage in the particular radiation environment of concern.

9.4.1 Ionization Chambers

A basic type of instrument used at accelerators to measure absorbed dose rates is the ion chamber. Such devices are used at high energy accelerators extensively. They rely on the collection of charge liberated by particles passing through a gas. Some detectors used in physics research now employ liquids for the ionization medium. A fortunate result of atomic physics is that the energy dissipation per ion pair, *W*, is nearly a constant over a number of gases and rather independent of type of charged particle as exhibited by Table 9.1.

Table 9.1 Values of the energy deposition per ion pair, *W*, for different gases[a] [Adapted from (Kn79).]

	W (eV/ion pair)	
Gas	**Fast Electrons**	**α- particles**
A	27.0	25.9
He	32.5	31.7
H_2	38.0	37.0
N_2	35.8	36.0
Air	35.0	35.2
O_2	32.2	32.2
CH_4	30.2	29.0

[a]The original data was obtained from Curran (Cu55).

Thus in a gas with a certain value of W (eV/ion pair), a charged particle depositing a certain amount of energy, ε (MeV) will liberate an electrical charge, Q_{elect} (Coulombs) according to

$$Q_{elect} = \frac{1.6\times10^{-13}\varepsilon}{W}. \tag{9.13}$$

The charge Q_{elect} is, then, collected by electrodes held at some voltage, V. The collected charge generates a small change in V, ΔV (volts), in accord with the relation,

$$\Delta V = \frac{\Delta Q_{elect}}{C} \tag{9.14}$$

where C is the capacitance of the total circuit (including that of the chamber) in units of Farads. For typical chambers, C is of the order of 10^{-10} Farads. Knoll (Kn79) gives many details of the processes that determine the size and form of the electrical signals that can be generated in a measurement. Such chambers can be operated either in a current, so-called "DC" [i.e., direct current] or **ratemeter**, mode, or in a **integration** mode in which the charge is integrated over some time period with the total charge collected, then digitized into pulses that represent some increment of absorbed dose or dose equivalent. In the ion chamber mode of operation, the applied voltage is sufficiently small so that gas multiplication (charge amplification) does not occur. In the most simple-minded approach, one might believe that for measurements in photon fields one could fill such a chamber with gases that "mimic" tissue and, with suitable calibration, convert the charge collected into absorbed dose. Such **tissue equivalent** gases range from complex mixtures to simply hydrocarbons, depending upon the accuracy of the representation of biological tissue that is desired. However, since ion chamber gases are in general much less dense than tissue, one must also capture the energy of the secondary electrons, which in the region of a few MeV have ranges of several meters in such gaseous material. It is thus necessary to use compensation techniques in which the solid material of the walls is chosen because of properties that match those of the gas.

This condition can be readily achieved by the use of any material having an atomic number close to that of the gas. The accuracy is sufficient for most practical purposes. Thus, aluminum and especially plastics, for example, are reasonably equivalent to tissue and air, at least for use in photon radiation fields. Such walls must be of thickness to establish **electronic equilibrium**. In this condition, the flux of secondary electrons leaving the inner surface of the wall is independent of the thickness. Table 9.2 gives the wall thickness needed to establish electronic equilibrium for photons of various energies.

Table 9.2 Thickness of ionization chamber walls required for establishment of electronic equilibrium[a] [Adapted from (Kn79).]

Photon Energy (MeV)	Thickness[b] (g cm^{-2})
0.02	0.0008
0.05	0.0042
0.1	0.014
0.2	0.044
0.5	0.17
1	0.43
2	0.96
5	2.5
10	4.9

[a]From (IC71).

[b]The thicknesses quoted are based on the range of electrons in water. The values will be substantially correct for tissue-equivalent ionization chamber walls and also for air. Half of the above thickness will give an ionization current within a few percent of its equilibrium value.

The measurement of absorbed dose is accomplished by application of the **Bragg-Gray principle**, which states that the absorbed dose D_m in a given material can be deduced (with suitable unit conversions) from the ionization produced in a small gas-filled cavity within that material as follows:

$$D_m = WS_m P\,, \tag{9.15}$$

where W is the average energy loss per ion pair in the gas, S_m is the ratio of mass stopping power, that is, the energy loss per unit density, (e.g., MeV/g cm^{-2}) of the material of interest, to that of the chamber gas, and P is the number of ion pairs per units mass formed. For D_m to be in grays (J kg^{-1}), W must be expressed in Joules per ion pair and P in ion pairs per kg.

For accelerator radiation fields that contain neutrons, or mixtures of neutrons with muons and photons, one is commonly able to use an ideal ion chamber to measure the absorbed dose, D, and determine the dose equivalent, H, by using the average quality factor, Q as follows [see also Eq (1.1)]:

$$H = QD. \tag{9.16}$$

Ion chambers with tissue equivalent walls have been used in this manner at many accelerators. The value of *Q* has to be determined by some other means such as those described later in this chapter; usually as a separate measurement. Awschalom described the use of such instruments at Fermilab (Aw72). These chambers, and their later versions, are filled with suitable gases and have tissue equivalent plastic walls. They have a net volume of about 3.4 liters. Current versions of these instruments have chambers produced commercially and are made of 4 mm thick walls of phenolic. They are filled with propane gas at atmospheric pressure and contain an electrometer encased in a sealed container. Several different ion chambers commonly used at Fermilab have been studied by Freeman and Krueger (Fr84). Their properties are briefly described in Table 9.3.

Table 9.3 Descriptions of ionization chambers used at Fermilab. The instruments designated "new" were produced after 1980 while those designated "old" were produced earlier. [Adapted from (Fr84).]

"Old" Chipmunk	A high-pressure gas-filled ionization chamber designed by Fermilab and built by LND, Inc. with 4 mm thick walls of tissue-equivalent plastic. The fill gas is 10 atmospheres of ethane. The chamber is enclosed in a protective box that contains a sensitive electrometer and associated electronics to measure the current output and convert it to the dose equivalent rate. Switch-selectable quality factors of 1, 2.5, or 5 are available. The instrument is equipped with a visible dose equivalent ratemeter and audible alarms. It provides a remote readout and capability for interface with radiation safety interlock systems.
"New" Chipmunk	These instruments are similar to the Old Chipmunk except for the use of phenolic-lined ionization chamber, filled with propane gas at atmosphere pressure and an electrometer encased in a sealed container. The reduced gas pressure was chosen for safety and the sealed container was provided to improve reliability over a larger range of temperature and humidity. The ion chambers were supplied by HPI, Inc. The latest versions of this instrument also allow for the selection of a quality factor of 10.
"Old" Scarecrow	A high-pressure ionization chamber with bare stainless steel walls filled with 10 atmospheres of ethane gas. The instrument is otherwise similar to the Old Chipmunk but with a fixed quality factor of 4 and capability to measure dose equivalent rates 100 times higher (up to 10 rem h^{-1}). A visible ratemeter, audible alarm, and remote readout capability are present as is the provision for interface to radiation safety interlocks.
"New" Scarecrow	The electronics and functionality is similar to that of the Old Scarecrow, but the ion chamber of the New Chipmunk is used.

Typically, such chambers are calibrated using photons and have a typical "quality factor" built in to the electronics. Such chambers are available either as line-powered fixed monitors or as hand-held survey instruments. The use of such instruments at accelerators must be done with the assurance that the instrument will respond correctly to the radiation field present. Neutron radiation fields are generally considered to be the most difficult in which to do this successfully. Höfert and Raffnsøe of CERN have made measurements of the response of various instruments, including tissue equivalent ion chambers (Hö80).

They were able to test such chambers, along with others (see discussion below), in neutron radiation fields having measured neutron energies ranging from thermal to 280 MeV. The neutron fields originated from reactor and radioactive sources, except that at 280 MeV, a neutron beam from the 600 MeV CERN Synchrocyclotron was used. Table 9.4 provides the results.

Table 9.4 Absorbed dose response and measurement errors for tissue equivalent ion chambers as a function of neutron energy. [Adapted from (Hö80).]

Neutron Energy (MeV)	Absorbed Dose Response (10^5 Coulombs Gy^{-1})	Error (%)
thermal	0.446	9.8
0.0245	0.404	12.1
0.1	0.622	6.1
0.25	0.806	7.1
0.57	0.885	5.4
1.0	0.885	5.4
2.5	0.993	6.1
5.0	1.179	5.2
15.5	1.370	5.2
19.0	1.664	12.1
280.0	0.389	10.1

The performance is reasonably independent of energy in the energy region that typically dominates the dose equivalent (approximately up to about 5 MeV).

Simple tests that have been conducted at Fermilab indicate that absorbed dose measured in muon fields is adequately understood using the γ-ray calibration of the instruments (Co87). These tests have involved comparison with direct measurements of the muon fluence using counter-telescope techniques, and typically are in agreement within about 10 per cent for the Fermilab-built instruments described previously. This is to be expected since muons at high energies behave as "minimum ionizing particles" whose loss of energy in matter proceeds, to first order, exactly as does that of electrons.

Practical problems encountered with such ion chambers are mostly those due to radiofrequency interference, pulsed radiation charged fields, and environmental factors such as temperature extremes and humidity. Cossairt and Elwyn (Co87) determined that air-filled, self reading pocket ion chambers of the type that are commonly issued to personnel to allow real-time monitoring of exposure to γ-rays, performed very well in *muon* radiation fields (measuring absorbed doses to within about $\pm$ 15 %). This is due to the fact that the ratio of muon stopping power in tissue to that in air for energies between 1 and 800 GeV is 1.07 $\pm$ 0.05 (St83).

9.4.2 Geiger-Müller Detectors

These instruments, among the oldest developed for the detection of radiation, are in conspicuous use at particle accelerators primarily with respect to detection and

measurement of induced activation and removable induced activity (contamination). In some instances such instruments can be used to identify prompt radiation fields. They are very rugged and remarkably insensitive to environmental effects such as temperature and humidity. However, the typical dead time of 100 μsec renders them to be generally useless in fields having high instantaneous rates.

9.4.3 Thermoluminescent Dosimeters (TLDs)

Swanson and Thomas (Sw90) and Knoll (Kn79) have provided discussions of the properties of TLDs. These dosimeters are an attractive alternative to photographic film particularly to monitor personnel exposures in β and γ radiation fields. They have also been found to be useful in measuring neutron radiation fields when used as a pair of ^{6}LiF and ^{7}LiF TLDs crystals in the same dosimeter. Such use exploits the fact that the $^{6}Li(n,\alpha)^{3}H$ reaction has a large thermal neutron cross section of 940 barns (see Section 9.5.1.2) while the $^{7}Li(n, \gamma)^{8}Li$ reaction cross section is only 0.037 barns for thermal neutrons. Since a TLD containing either ^{6}Li and ^{7}Li has a comparable efficiency for photon or muon radiation, measurement of the response of the two detectors can, then, be used to determine the dose equivalent due to thermal neutrons in the presence of photons or muons. These reactions provide tools to use in the detection of fast neutrons if moderation is supplied, as will be discussed later.

TLDs operate on the principal that some of the radiation liberated by the ionizing particle is "trapped" in band gaps in the crystal lattice. The process is well described by Knoll (Kn79). In particular, ionization elevates electrons from the valence to the conduction band where they are then captured by a "trapping center". At room temperatures, there is only a small probability per unit time that such "trapped" electrons will escape back to the conduction band from the valence band. Thus exposure to radiation continuously populates the traps. "Holes" are similarly trapped in the valence band. When readout of the dose is desired, the crystal is heated and this thermally excites the electrons and holes out of the traps. This process is accompanied by the emission of light that can then be measured as a so-called "glow curve". A number of other materials can function as TLDs: notably $CaSO_4$:Mn, CaF_2, and CaF_2:Mn. These materials have properties that can be optimized for particular applications. The latter is particularly useful for environmental monitoring purposes, where extraordinarily high sensitivity is required. The large numbers of trapped electrons and holes per unit of dose permits sensitivity to absorbed doses as small as 2×10^{-5} rads. LiF "fades" over time to a lessor degree than most of the other materials at room temperature and its average atomic number is very close to that of tissue, so it is particularly useful for personnel dosimetry.

TLDs can give valid results for fields as high as 100 rads. Higher doses can be measured under certain conditions if one takes care to use crystals calibrated in the intense radiation fields since linearity of the response breaks down in the high dose region. These devices become superlinear. Also, TLDs are not generally susceptible to dose rate problems.

9.4.4 Nuclear Track Emulsions

This discussion is summarized from that of Swanson and Thomas (Sw90). For many years, thin (≈ 25 micron) emulsions (NTA) have been used for personal dosimetry in fast neutron fields. The technique is based upon detection of tracks left by proton recoils in the film. The energy range for which these dosimeters are effective is from roughly 0.5 to 25 MeV because below that range the tracks are too short to be read out, while above it there are too few tracks because the (n, p) cross section (elastic scattering, mostly) decreases with energy. However, this energy range is the one that often results in significant neutron dose equivalents at accelerators. The singular important problem with NTA is that the latent image fades and leads to underestimates of the dose equivalent. The fading time can be a short as two weeks. Extreme efforts to keep out the moisture, and experience in dry climates give some indication that this problem can be overcome.

Höfert (Hö84b), as has Greenhouse, et al. (Gr87), has given a good summary of experience with this dosimeter at accelerators. The dose equivalent range from about 10 mrem to a few hundred mrem is that for which this dosimeter can be expected to perform acceptably. Any technique based upon track formation should not be dependent upon dose rate effects.

9.4.5 Track Etch Dosimeters

Swanson and Thomas (Sw90) have discussed the use of such dosimeters. In these detectors, the passage of a charged particle through a dielectric material will result in a trail of damaged molecules in the material. These tracks can be made visible upon etching in a strong acid or base solution. The tracks will be etched at a faster rate than the undamaged portions of the material. As with nuclear emulsions, there is a minimum detectable track length that sets a threshold of about 0.5 MeV on the neutron detection. Such detectors have been reviewed extensively by Griffith and Tommasino (Gr90). Mica, Lexan, and other materials are suitable for this purpose and electronic methods of readout are becoming available.

9.4.6 CR-39 Dosimeters

Swanson and Thomas (Sw90) have provided a discussion of applications of such dosimeters at accelerators. This material has largely replaced NTA as a film dosimeter. It is also a "track detector". It is a casting resin, originally developed for use in eyeglass lenses that is transparent and is thermoset, rather than thermoplastic. It is the most sensitive of the track detectors and registers recoil protons up to 15 MeV and down to about 0.1 MeV. It is read out either chemically or electrochemically. The lower limit of detection appears to be improved over NTA and Track-Etch (Lexan). There are about 7×10^3 tracks cm^{-2} rem^{-1}, which appears to be adequate. The sensitivity may be as much as a factor of two lower in high energy spectra. Fading appears to be insignificant.

However, natural radon gas can contribute to background readings and the angle of incidence is important. Greenhouse et al. (Gr87) have experimented with these dosimeters in an accelerator environment with "mixed" results. However, the general conclusion of practitioners is that this material is promising.

9.4.7 Bubble Detectors

The use of these detectors at accelerators has also been discussed by Swanson and Thomas (Sw90). The bubble damage polymer detector is a relatively new dosimeter that is similar to a bubble chamber in that a liquid whose normal boiling point is below room temperature is kept under pressure. When the pressure is released bubbles form along the path of a charged particle that has traversed it. To enhance the effect, superheated droplets of a volatile liquid are dispersed in a gelatinous medium. There are two types of these detectors that have been developed; one type by Apfel (Ap79) and the other type by Ing (In84). The polymer or gel is supplied in a clear vial. When a neutron interacts in the sensitive material, a bubble is created that expands to optically visible dimensions and can thus be counted. There is no angular dependence but temperature effects must be considered. The Ing detector presently exhibits constant response over the range 15 ^{o}C < T < 35 ^{o}C. The material can be tailored to match a chosen neutron energy threshold that can be as low as 10 keV or less. Indeed, sets have been prepared with arbitrary thresholds of 0.010, 0.100, 0.500, 1, 3, and 10 MeV. The range of sensitivity can be adjusted to be between 1 and 30 bubbles per mrem, or larger, in a volume of about 4 cm^3 and the physical mechanism is not readily sensitive to dose rate effects. Disadvantages include a high unit cost, and the fact that once the vial is opened it is only good for a few weeks of dose integration. The materials have been successfully used at accelerator facilities. These detectors could not be expected to give accurate results in high dose rates.

One can see that no single commercial instrument "solves all problems" simultaneously, especially for neutron fields. The practitioner is encouraged to utilize a variety of instruments, including some of the special techniques discussed below to fully understand the radiation fields.

9.5 Specialized Detectors

9.5.1 Thermal Neutron Detectors

Although thermal neutrons are not commonly the major source of neutron dose equivalent at particle accelerators, they are of considerable importance in accelerator radiation protection because of the ability to moderate the fast neutrons (as we shall see below). Furthermore, because some of the most prominent thermal neutron detectors rely upon radioactivation (by neutron capture) as the detection mechanism, they have the advantage that the response is entirely independent of dose rate effects and hence free of dead-time effects. An excellent discussion, summarized here, on thermal neutron detectors is given by Knoll (Kn79).

At the outset, there are some general features concerning thermal neutrons that need to be recalled. The kinetic energies of thermal neutrons have the familiar relationship as a function of temperature, given by the Maxwell-Boltzmann distribution:

$$f(E) = \frac{2\pi}{(\pi kT)^{3/2}} E^{1/2} \exp\left\{-\frac{E}{kT}\right\}, \tag{9.17}$$

where $f(E)$ is the fraction of neutrons (or gas molecules) of energy E per unit energy interval, k = 1.38 x 10^{-23} J $^{o}K^{-1}$ or 8.62 x 10^{-5} eV $^{o}K^{-1}$ (Boltzmann constant) and T is the absolute temperature of the gas (^{o}K). The most probable energy, E_{mp}, is given by

$$E_{mp} = kT, \tag{9.18}$$

while the average energy at any given temperature, $\langle E \rangle$, is

$$\langle E \rangle = \frac{3}{2} kT. \tag{9.19}$$

At room temperature, T = 293 ^{o}K, so that the most probable energy is 0.025 eV. The most probable velocity, $\langle v \rangle$, at T = 293 ^{o}K (since thermal neutrons are decidedly nonrelativistic!) is given by

$$\frac{1}{2} m \langle v \rangle^2 = kT, \text{ so that } \langle v \rangle = 2200 \text{ m s}^{-1}. \tag{9.20}$$

As the neutron energy increases above the thermal value (up to about 1 keV), unless there are resonances present in the cross section, the absorption cross section, σ, has been found to be approximately described by the relation

$$\sigma \propto \frac{1}{\sqrt{E}} \propto \frac{1}{v}, \tag{9.21}$$

that is known as the **1/*v* law**. Thus, within the limits of validity of the 1/v law, one can scale from the tabulated "thermal" cross section, σ_{th}, as follows:

$$\sigma(E) = \sigma_{th} \sqrt{\frac{E_0}{E}}. \tag{9.22}$$

Several different nuclear reactions that are initiated by thermal neutrons are used as the basis of detectors. They all involve particular target nuclei and thus the detector materials sometimes depend upon isotopically separated materials to enhance the effectiveness.

9.5.1.1 Boron-10

The $^{10}B(n, \alpha)^{7}Li$ reaction is exothermic, having a *Q*-value [see Eq. (4.1)], Q_v, of 2.792 MeV, and leads either to the ground state of ^{7}Li or its first excited state at 0.482 MeV. The latter occurs for about 94 % of the time when thermal neutrons are incident. Thus, for the dominant transition to the excited state, the reaction imparts about 2.31 MeV to the reaction products. This energy is much larger in energy than is that of the incoming thermal neutron. Since energy and momenta must be conserved, for the dominant excited state branch the energy of the alpha particle, $E(\alpha)$, is 1.47 MeV and $E(^{7}Li)$ = 0.84 MeV. This is because the following must hold:

$$E(^{7}Li) + E(\alpha) = 2.31 \text{ MeV}, \tag{9.23}$$

due to energy conservation for the excited state branch, if one neglects the very small kinetic energy of the incident thermal neutron. Also,

$$[2m(^{7}Li)E(^{7}Li)]^{1/2} = [2m(\alpha)E(\alpha)]^{1/2} . \tag{9.24}$$

holds due to conservation of momentum if the two reaction products emerge in opposite directions. The very small momentum of the thermal neutron is ignored and one recalls that, nonrelativistically, $p^2 = 2mE$, where *m* denotes the rest mass of the particle.

The excited state subsequently decays by emission of a photon. For this reaction, at 0.025 eV, σ_{th} = 3837 barns. The natural abundance of ^{10}B is 20 % compared with 80 % for the other stable isotope, ^{11}B (Se81). The large natural abundance of the crucial isotope makes this reaction very favorable for thermal neutron detection. In addition, material enriched in ^{10}B is readily available. Also the reaction products, and thus their deposited energies, being of short range, are contained in "reasonable" detector configurations. Figure 9.1 gives the cross sections as a function of neutron energy for several of the thermal capture reactions described here, including this one. It is useful that the Boron-10 reaction has a rather featureless cross section and obeys the $1/v$ law quite well even up to approximately an energy of approximately 0.5 MeV.

This reaction has been used principally in BF_3 gas in proportional tubes. Proportional counters are somewhat similar in concept to ionization chambers except that the applied electric fields are of sufficient strength to accelerate the initial electrons liberated by the ionization to energies above the thresholds for liberating additional secondary electrons. In typical gases at one atmosphere, this threshold is of the order 10^6 volts/meter. Under proper conditions, the number of electrons generated in this process can be kept proportional to the energy loss but the number of electrons released (and hence the size of the signal) can be "amplified" by a "gain" of many thousands. In proportional chambers, the region in which these secondary electrons are released is kept small compared to the chamber volume. If the voltage is raised beyond these conditions, then proportionality is lost and the counter enters the Geiger-Mueller mode. Knoll (Kn79) has given a detailed

exposition on proportional chambers and the gas multiplication process. BF_3 is the best of the boron-containing gases as a proportional counter gas because of its "good" properties as a counter gas and also because of the high concentration of boron in the gas molecule. Typical BF_3 tubes operate at 2000 to 3000 volts potential with gas gains of 100-500. An enriched (96%) BF_3 tube can have an absolute detection efficiency of 91 % at 0.025 eV dropping to 3.8 % at 100 eV for neutrons incident upon it. Alternatives with somewhat better gas properties (and cleaner signals) have been achieved by using boron-lined chambers with other gases that have better properties in proportional chambers.

9.5.1.2 Lithium-6

The reaction of interest is $^6Li(n, \alpha)^3H$. For this reaction, Q_v = 4.78 MeV. The process leads only to the ground state of ^3H. As discussed in connection with the $^{10}B(n, \alpha)^7Li$ reaction, conservation of energy and momentum can be shown to yield the result that E (^3H) = 2.73 MeV and E (α) = 2.05 MeV. For incident thermal neutrons, σ_{th} = 940 barns (Se81). The natural isotopic abundance of ^6Li is about 7.5 %. Figure 9.1 includes the cross section of this reaction as function of neutron kinetic energy. The cross section exhibits a significant resonance at about 3 x 10^5 eV. The apparent disadvantage of the "small" thermal cross section is offset by the higher Q -value and resultant larger signals.

For use in gas counters, no equivalent to the convenience of BF_3 gas has been found for this reaction. Instead, ^6Li has been successfully added to scintillators. With the addition of a small amount (< 0.1 % of the total atoms) of europium to LiI [LiI(Eu)], the light output is as much as 35 % of that of a comparable size NaI(Tl) crystal. Such scintillators have a decay time of approximately 0.3 μs. Of course, ^6LiF is also in prominent use as a TLD and employs the same nuclear reaction. The TLD can be used in high dose rates, since no instantaneous readout is involved.

9.5.1.3 Helium-3

This nuclide, gaseous at room temperature, is used through the reaction $^3He(n, p)^3H$. The Q-value is 0.765 MeV so that, as for the other reactions, E (p) = 0.574 MeV and E (^3H) = 0.191 MeV for incident thermal neutrons. For this reaction, σ_{th} = 5327 barns (Se81). Although this isotope of helium can be used directly as a detector gas, it has the disadvantages that the natural abundance is only 0.000138 %, which renders enriched ^3He to be rather costly. Also some of the energy can escape the sensitive volume of a detector or reasonable size because of the relatively long range of the proton. Again, the cross section as a function of energy is given in Fig. 9.1. As seen, the cross section is quite "well-behaved". ^3He is a reasonable gas for proportional chambers; however no compounds are available since it is a noble gas. In sufficient purity it will work as an acceptable proportional counter gas. Because a proton is the reaction product instead of the short range α-particle, "wall effects" (i.e., effects in which some energy escapes the

counting gas volume) may be somewhat more severe than for BF_3. However, these tubes can be operated at much higher pressures than can BF_3 and can thus have enhanced detection efficiency compared to the former.

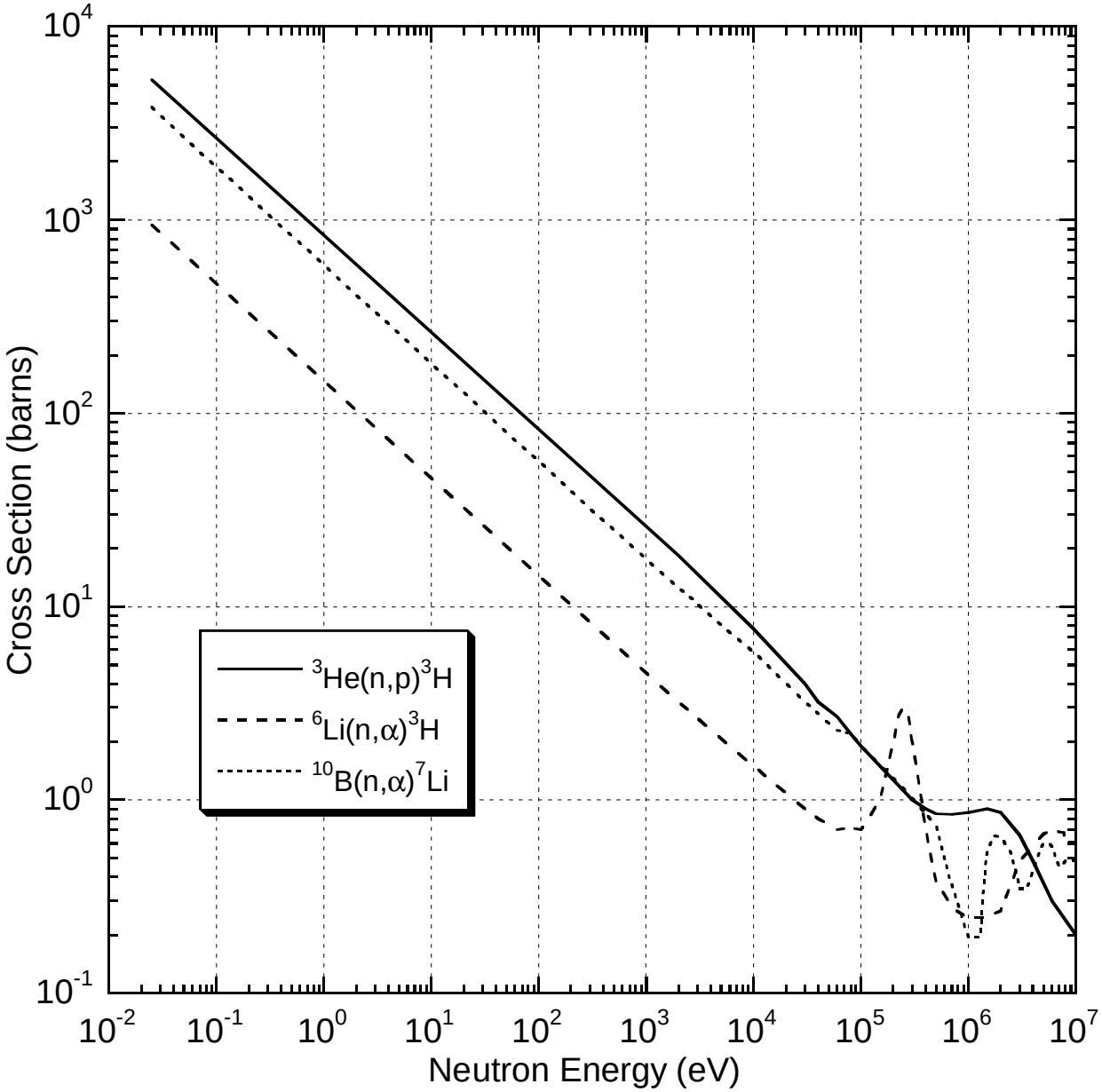

Fig. 9.1 Cross section versus neutron energy for some reactions of interest in neutron detection. [Adapted from (Kn79).]

9.5.1.4 Cadmium-113

The discussion would be incomplete without discussing cadmium. Averaged over the naturally occurring isotopes of cadmium, the thermal neutron capture reaction $^{A}Cd(n,\gamma)^{A+1}Cd$ has a cross section σ_{th} = 2450 barns. More spectacularly, the reaction $^{113}Cd(n,\gamma)^{114}Cd$ has a value of σ_{th} = 19910 barns (Se81). ^{113}Cd has a natural abundance of 12.2 %. Thus, even without using enriched material, the thermal neutron cross section is large. This element is not used directly in the detector medium. Rather, it is used to shield other detectors from thermal neutrons, especially enriched, because its large cross section has the effect of essentially eliminating all neutrons less than about 0.4 eV. Hence, one can do measurements with and without the Cd inside of some moderator and have a very clear understanding of the thermal component.

9.5.1.5 Silver

Awschalom was able to use thermal neutron capture on silver as a basis of a moderated detector (Aw72). As it occurs in nature, silver has two stable isotopes which both capture thermal neutrons via the (n, γ) process; ^{107}Ag (51.8% abundance, σ_{th} = 40 barns) and ^{109}Ag (48.2 % abundance, σ_{th} = 93.5 barns). The average value of σ_{th} is 63.6 barns (Se81). While the cross sections are not as large as those of some of the other reactions discussed, the material is readily available and enrichment is not needed. The detector which utilized these capture reactions was a moderated one (see below) in which the output of a Geiger-Mueller tube wrapped with silver that sensed the capture γ-rays was compared with an identical tube wrapped with tin (average mass number = 118.7). Tin has an average value of σ_{th} = 0.63 barns and is thus comparatively insensitive to thermal neutrons. The tin-wrapped tube was then used to subtract background due to muons, photons, etc.

9.5.2 Moderated Neutron Detectors

As seen, many neutron reactions tend to have much smaller cross sections in the MeV region than they have in the "thermal" region. At an early date following the discovery of the neutron, it was observed that surrounding a thermal neutron detector with hydrogenous materials enhance detection rates exhibited by a "bare" thermal neutron detector placed in the same radiation field. The reason this occurs with hydrogenous materials is because in nonrelativistic elastic scattering, as we have seen before, the fraction of the incident energy, E_o, that can be transferred to the target nucleus after a collision where the target nucleus recoils at angle θ, is determined by conservation of momentum and energy to be given by

$$\left(\frac{\Delta E}{E_o}\right) = \frac{4M\cos^2\theta}{(1+\mathrm{M})^2}, \tag{9.25}$$

where M is the mass of the target nucleus in units where the mass of the neutron is unity. The energy that can be transferred in the reaction is maximized in the head-on collision ($\theta = 0$) and has its maximum value (1) when $M \approx 1$ (hydrogen). Even for a nucleus as light as ^{12}C, the quantity $(\Delta E/E_o)_{max}$ is only 0.28.

One might, naively, expect that the detection efficiency to improve with the thickness of the moderator. However as the moderator thickness increases, the probability that a given neutron will actually ever reach the detector decreases. Fig. 9.2 illustrates these tradeoffs qualitatively. In general, the optimum thickness will, for moderators such as polyethylene, range from a few centimeters for keV neutrons to several tens of centimeters for MeV neutrons. Furthermore, for any given thickness, the overall counting efficiency as a function of energy will tend to show a peak at some energy determined by the thickness.

9.5.2.1 Spherical Moderators, Bonner Spheres, and Related Detectors

Bramblett, Ewing and Bonner employed spherical moderators to obtain low resolution neutron spectra (Br60) using a technique that has become known as the **Bonner sphere technique**. In this technique moderating spheres of different diameters surrounding a thermal neutron detector of some type are placed in a given radiation field. The normalized relative (or absolute) responses are, then, indicative of the neutron energy spectra. As one might expect, the determination of the efficiency of each sphere as a function of energy is a rather complicated matter, and such response functions have been calculated, using techniques such as the Monte Carlo method, by a number of authors over the years since this method was invented. Hertel and Davidson (He85) have calculated the response functions for spheres that comprise the "standard" set of diameters. Other response functions, perhaps more accurate in neutron fields of higher energies, have been reported by Awschalom and Sanna (Aw85). The response functions are dependent upon detector size as well as upon moderator thickness and density. The density is typically 0.95 g cm^{-3} for polyethylene. The results of Awschalom and Sanna are given in Fig. 9.3 for cylindrical LiI(Eu) detectors of lengths equal to their diameters which are each 1.27 cm (0.5 inch).

Most of the efficiency calculations have been made for ^{6}LiI(Eu) scintillators, but also can be used for ^{6}LiF TLD dosimeters. They cannot, in general, be used for other thermal neutron capture reactions used to detect thermal neutrons as the neutron cross section needed for the calculation of the responses will differ. As one can see, the larger detector readily gives a higher efficiency response at the higher energies as intuitively expected from the enhanced detector volume. There are other sets of response functions extant. Experimental verifications of the details of these response functions are rather rare because of the difficulty of the measurements. Kosako et al. (Ko85) have successfully verified some of the important response functions using a neutron time-of-flight technique in the especially difficult keV energy region of neutron energy. A Bonner sphere determination of the neutron spectrum is comprised of a set of measurements of the responses for the different spheres of radius r, C_r, where r has the discrete values

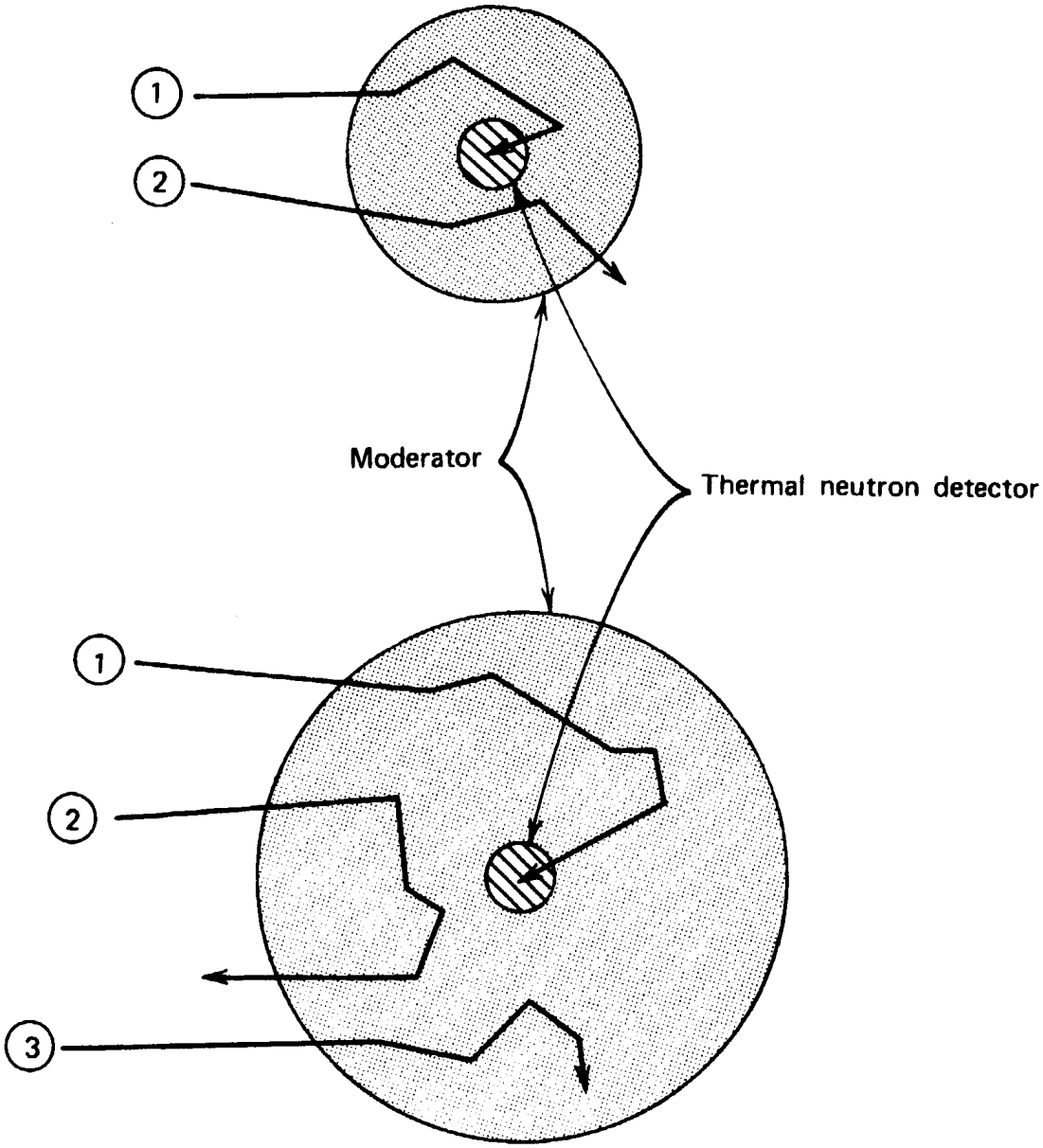

Fig. 9.2 Schematic representation of neutron histories in moderated detectors. The small thermal neutron detector at the center is shown surrounded by two different thicknesses of moderator material. Histories labeled **1** represent incident fast neutrons that are successfully moderated and detected. Those labeled **2** are partially or fully moderated, but escape without reaching the detector. History **3** represents those neutrons that are parasitically captured by the moderator. Larger moderators will tend to enhance process **3** while reducing process **2.** [Reproduced from (Kn79).]

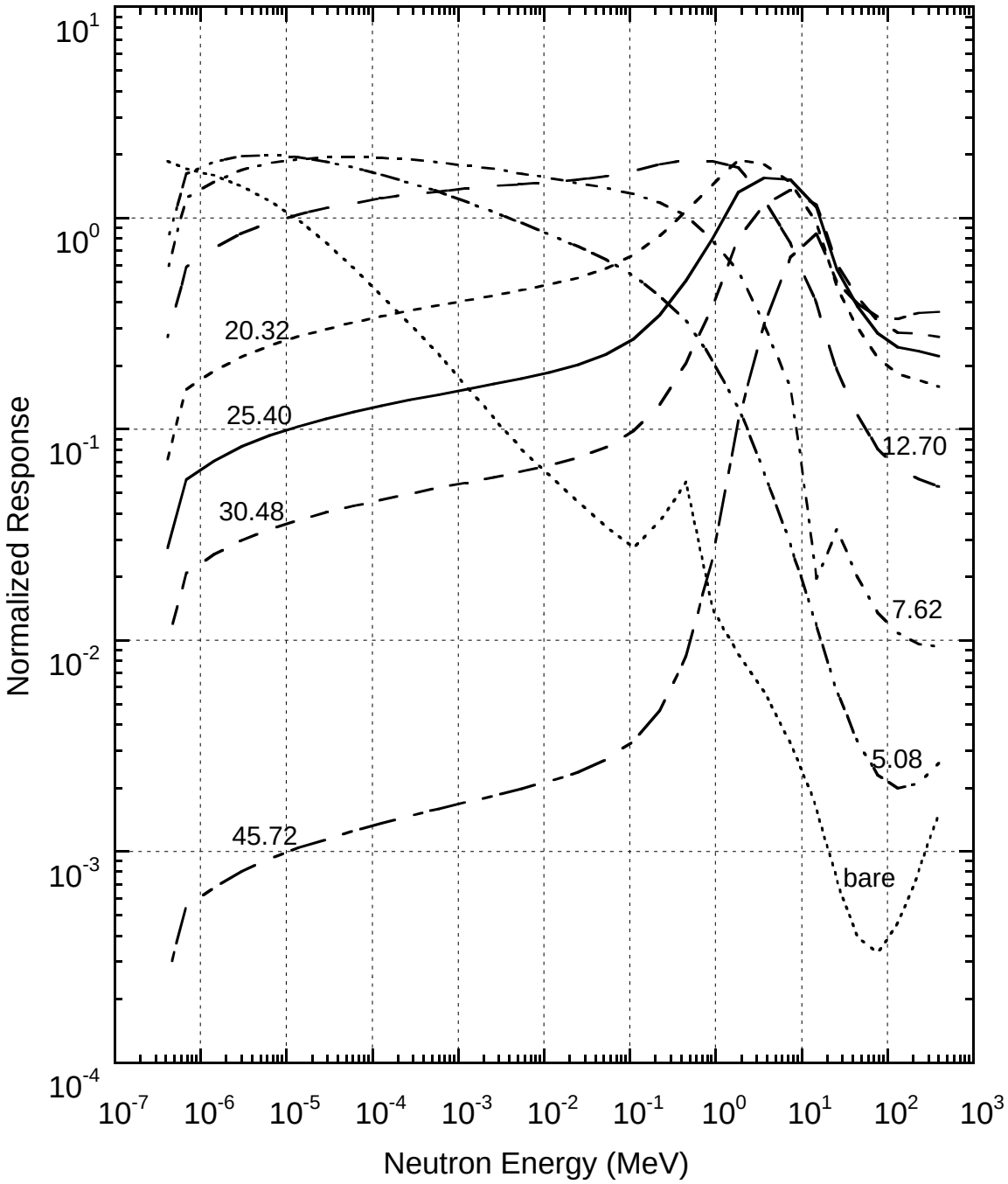

Fig. 9.3 The calculated responses for the bare 12.7 mm diameter LiI detector and for the same detector inside 5.08, 7.62, 12.7, 20.32, 25.4, 30.48, 38.1, and 45.72 cm diameter spheres as a function of neutron energy. The detector is a cylinder having a length equal to its diameter [Adapted from (Aw85).]

based on the available set. Such responses, ideally, are given by,

$$C_r = \int_0^\infty \frac{dN}{dE} R_r(E) dE \,, \tag{9.26}$$

where *dN/dE* is the differential neutron flux density (the neutron spectrum) and $R_r(E)$ is the energy-dependent response function for the sphere of radius *r*. One measures C_r and knows $R_r(E)$ with the objective of determining *dN/dE* by **unfolding** the spectrum. In practice, one works with a discrete approximation to the integral;

$$C_r = \sum_i \frac{dN}{dE_i} R_r(E_i)\Delta E_i , \tag{9.27}$$

where the index, *i*, labels each member of the set of "energy groups" used. The unfolding procedure is a difficult mathematical problem that, unfortunately, suffers from being underdetermined and mathematically ill-conditioned. One has as many as "unknowns" as one has energy groups, with typically only 8 or 9 measurements to determine the response. Commonly 31 energy groups are used in an attempt to achieve "reasonable" energy resolution in the results. A variety of numerical techniques have been developed to do the unfolding.

Prominent codes in use at accelerators include BUNKI (Lo84), LOUHI (Ro80), and SWIFT (OB81). The first uses an iterative recursion method and the second uses a least squares fitting procedure with user-controlled constraints. One essentially starts with an "educated guess" at the spectrum and iterates to fit the responses. As we have seen, a 1/*E* spectrum is a good starting point for an accelerator spectrum. SWIFT is based upon a somewhat different principle; it is a Monte Carlo program that makes no *a priori* assumptions on the spectrum and can thus provide a "reality check" on results using the other two. It has the disadvantage in that it is known to sometimes produce nonphysical peaks in the unfolded spectrum. In general, the codes agree best with each other for those properties that are determined by integrating over the spectrum such as the average quality factor, total fluence, and total absorbed dose and dose equivalent. Typical spectra obtained from such unfolding procedures have been reported at a number of laboratories. Fermilab results have been summarized in (Co88) and are, in general, similar to those obtained at other laboratories. Further discussion of examples of neutron measurements is provided in Chapter 6.

It is sometimes important to verify the reasonableness of the unfolded spectrum. Comparisons can be made with known spectra from radioactive sources such PuBe or AmBe and such comparisons have been made in, for example, (Co88). Sometimes, the normalized responses, C_r, can be directly used to check the reasonableness of the unfolded spectrum. For example, this was done for measurement in the labyrinth discussed in connection with Fig. 6.7 and for the iron leakage measurements described in connection with Fig. 6.8. The results are shown in Fig. 9.4 and Fig. 9.5. In Fig. 9.4 the labyrinth responses are compared with the sphere responses for a pure thermal neutron spectrum. The enhanced responses for the intermediate-sized spheres indicate the somewhat more energetic unfolded neutron spectrum that was observed. For the iron leakage spectrum (Fig. 9.5), one can see evidence for the "softening" of the spectrum after the concrete was added. Other verifications, of course can be obtained using entirely independent measurement techniques.

In the use of ^{6}LiI(Eu) scintillators for such detectors in mixed fields, there are situations in which the signals from photons and/or muons can overwhelm the neutron signal. Awschalom and Coulson (Aw73) have developed a technique in which the ^{6}LiI(Eu) is surrounded by plastic scintillator. The physical configuration of such a phoswich detector, and a typical pulse height spectrum obtained by use of this detector in a long exposure to environmental neutrons are given in Figs. 9.6 and 9.7. The same detector

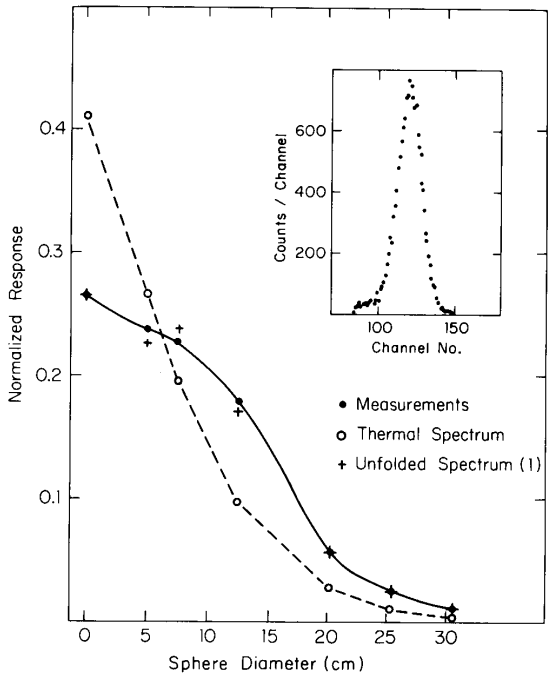

Fig. 9.4 Normalized response from the detector as a function of spherical moderator diameter. The solid circles are the measurements within the second leg of the labyrinth shown in Fig. 6.7. The open circles represent calculated results assuming a purely thermal spectrum while the crosses are the results for the neutron energy spectrum unfolded using the program SWIFT. The solid and dashed curves are drawn to guide the eye. The inset shows a typical gated spectrum of the pulse heights in the ^{6}LiI(Eu) phoswich detector described in the text. [Reproduced from (Co85b).]

was used to produce the pulse-height spectrum shown in the inset in Fig. 9.4. In this technique, a "fast" discriminator is set to respond to the 2-3 nanosecond decay time of the plastic scintillation signal while a "slow" discriminator is set to respond to the 1.4 μsec decay time of the crystal. Selecting the slow counts not accompanied by fast counts clearly gives superior discrimination against non-neutron events from environmental radiation (e.g., cosmic ray muons) which produces coincident pulses in both the crystal and the plastic scintillator.

In performing Bonner sphere measurements in neutron fields that are suspected of being nonuniform in space, it may be necessary to measure C_r over the set of spheres individually because arranging them in an array may result not only in undesired "cross-talk" between the moderators but also in the need to make corrections for the non-uniformities of the radiation field.

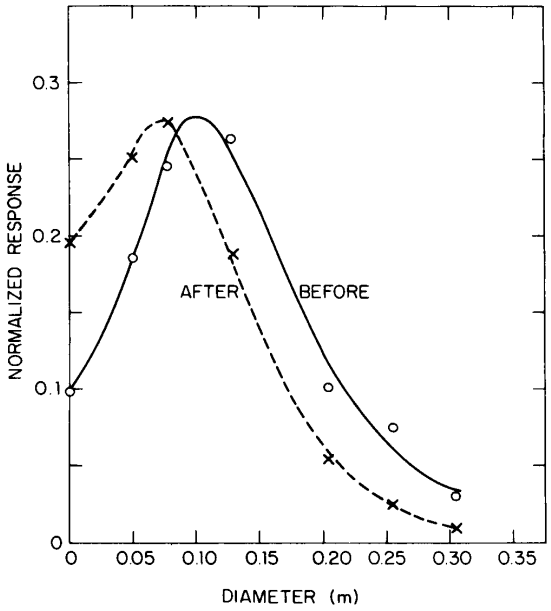

Fig. 9.5 Normalized detector response as a function of spherical moderator diameter for the situation presented in Fig. 6.8. The open circles are the measurements **before**, and the X's are the measurements **after** the placement of the additional concrete shielding. [Reproduced from (El86).]

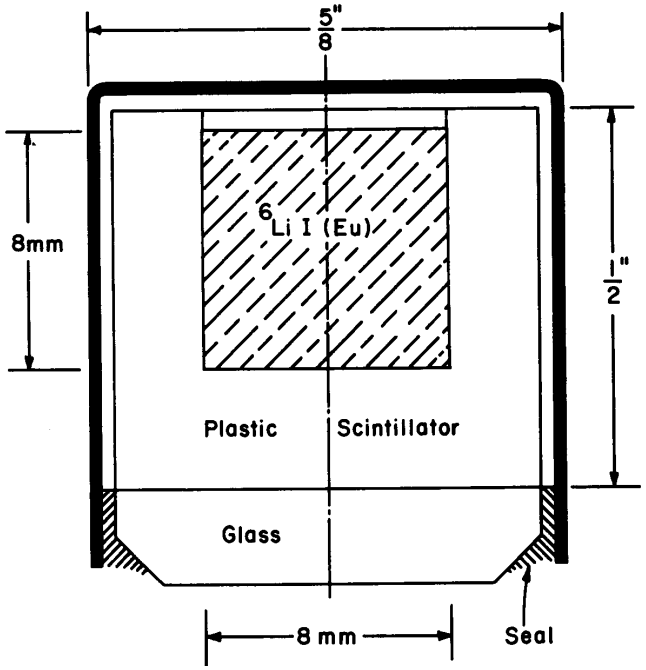

Fig. 9.6 Cross section of 8 mm x 8 mm phoswich. [Reproduced from (Aw73).]

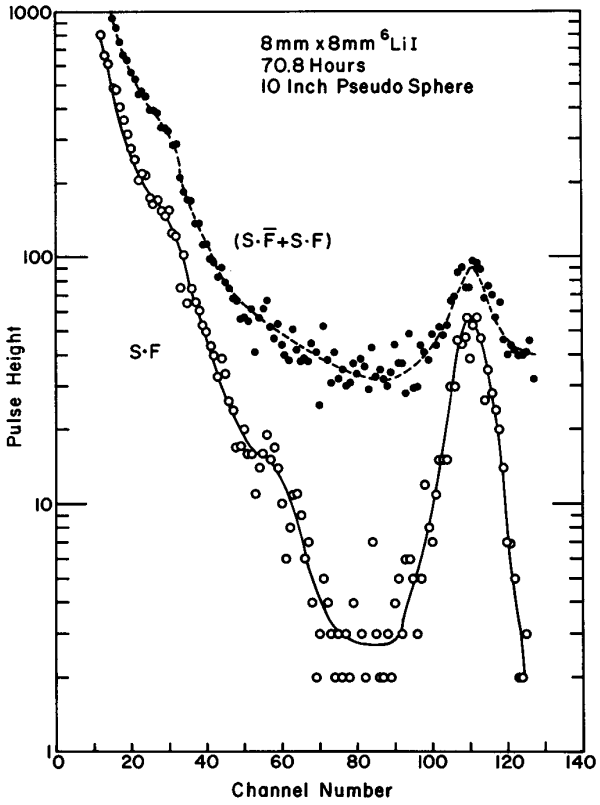

Fig. 9.7 Pulse height spectra obtained using the phoswich shown in Fig. 9.6 in a natural background radiation field. The upper curve is spectrum of all slow pulses (slow with fast and slow without fast). The lower curve is spectrum of slow pulses not accompanied by fast pulses, e.g., "neutrons". [Reproduced from (Aw73).]

Since accelerator neutron fields are often quite similar to each other, it was noticed that the choice of a single moderator size might well offer the opportunity to construct a **rem-meter**. Such an instrument uses a given sphere response function particularly well matched to energy dependence of the fluence per dose equivalent conversion factor. The standard implementation of this is in the development of the Andersson-Braun detector (An62), which uses a BF_3 detector. The usage of such counters was reviewed by Thomas and Stevenson (Th88). Generally, the 25.4 cm (10 inch) diameter polyethylene sphere has been selected because its response curve provides the best match to the curve of fluence-to-dose equivalent. Höfert and Raffnsøe (Hö80) have measured the dose equivalent response of such an instrument as a function of neutron energy. Their results are given in Table 9.5. Generally, commercial versions of this instrument operate in the proportional counter mode. This renders them somewhat suspect in accelerator fields with high instantaneous dose rates that arise because of the small duty factor due to pulsed beams. A similar detector has been developed by Hankins and employed ^{6}LiI(Eu) as the detector (Ha62). Hankins obtained the response shown in Fig. 9.8 that includes a comparison with the "Inverse of the Radiation Protection Guide (RPG)" curve that embodies the relative dose equivalent delivered per neutron as a function of neutron energy. In the keV region, comparisons are difficult and there is some evidence that the

detector overresponds considerably. However, the matching was verified at thermal neutron energies. Leake (Le68) has developed an alternative detector of this general type. In this detector a ^{3}He proportional counter is used in a 20.8 diameter sphere to reduce background due to photons along with a cadmium filter against thermal neutrons.

It is claimed that this detector is effective in photon fields as high as 20 Roentgens per hour. There are concerns that above 10 MeV this type of instrument seriously underestimates neutron dose equivalent rates.

Table 9.5 Dose equivalent response and measurement errors for a 25.4 cm diameter polyethylene moderating sphere as a function of neutron energy. [Adapted from (Hö80)]

Neutron Energy (MeV)	Dose Equivalent Response (10^5 Coulombs Sv^{-1})	Error (%)
thermal	0.349	10.0
0.0245	3.209	12.1
0.1	1.335	6.8
0.25	1.082	6.1
0.57	0.923	5.2
1.0	0.745	5.2
2.5	0.784	6.1
5.0	0.653	5.2
15.5	0.348	5.2
19.0	0.445	12.2
280.0	0.157	10.1

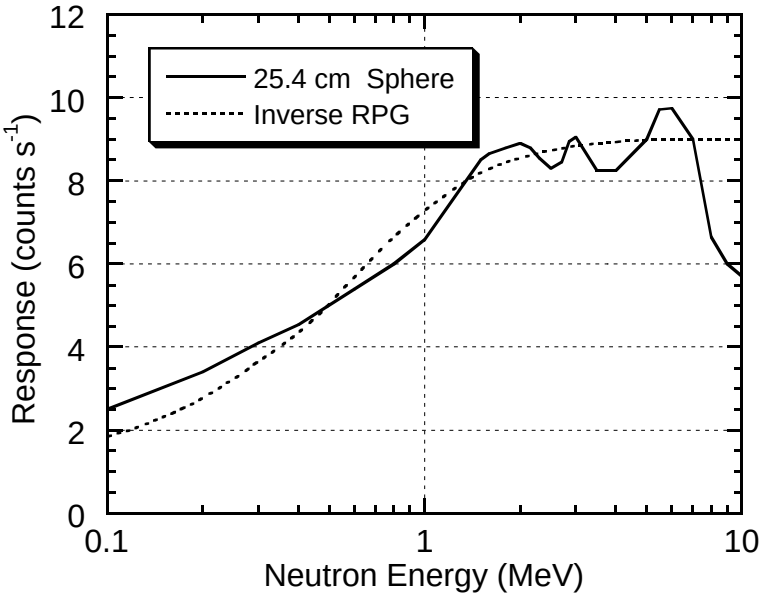

Fig. 9.8 Sensitivity of detector comprised of a 25.4 cm (10 in.) diameter moderating sphere surrounding a 4 mm x 4 mm LiI scintillator in counts s^{-1} at 40 cm distance from a source of 10^6 neutrons s^{-1}. Also shown is the relative dose equivalent per neutron labeled as "Inverse of RPG curve". At thermal energies, the response was measured to be 0.227 compared with a value of 0.225 for the "Inverse of RPG" curve (see text). [Adapted from (Ha62).]

It is not necessary, for radiation protection purposes, that a "spherical" moderator be an exact sphere. Awschalom et al. (Aw72) measured the responses of three polyethylene moderators; a sphere, an octagon of revolution, and a cylinder. The sphere had a diameter of 25.4 cm and the sizes of the other moderators were chosen to have the same volume as the sphere. It was found that the alternative moderators have a response indistinguishable from that of the sphere as a function of polar angle of the detector with respect to the axis of revolution. Such pseudospheres and cylinders are desirable because they are cheaper to machine than are spheres. The results the measurements of Awschalom et al. are shown in Fig. 9.9

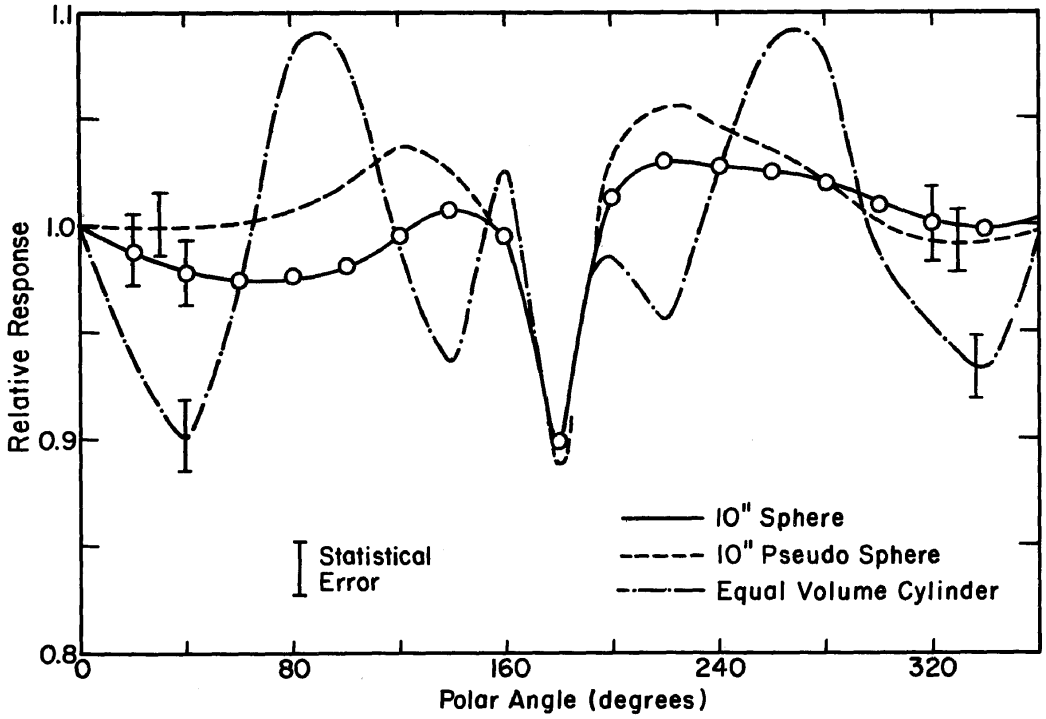

Fig. 9.9 Relative neutron detection efficiency of three different moderators with a 4 x 4 mm^2 ^{6}LiI(Eu) detector at the center. The efficiencies are plotted as a function of the polar angle. The zero angle is measured along the axis of the light pipe. [Adapted from (Aw72).]

9.5.2.2 Long Counters

Another type of moderated neutron detector that has been used extensively is the **long counter.** The idea is to adjust the configuration of moderators around some thermal neutron detector in such a manner as to assure that the detection efficiency plotted as a function of neutron energy is a straight line. It has been found over the years that the best detector is a cylinder of moderating materials surrounding a thermal neutron detector (also cylindrical) on the axis. Since a cylindrical detector is desired, the BF_3 proportional counter is the most popular. One end of the cylinder "views" the neutron source for best

results. Hanson and McKibben (Ha47) were the pioneers of the technique. An improved version, which has rather widespread use, is that developed by DePangher and Nichols (DeP66). Figure 9.10 shows the layout of this detector. The length and diameter are both approximately 41 cm and the mass is about 45 kg. The neutrons are to be incident on the "front" face.

Perhaps the best calibration data on this device is that of Slaughter and Rueppel (Sl77). They used filtered beams from a reactor ($E_n \approx$ keV) as well as monoenergetic neutron beams from (p, n) and (d, n) reactions at accelerators to cover the energy range from 10 keV to 19 MeV. An average of about 3.5 counts/(n cm^{-2}) sensitivity was reported over this energy domain. A similar detector has been used to conduct studies of skyshine at Fermilab [(Co85c) and (El86)]. The large peak in the pulse-height spectrum of the BF_3 tube from thermal neutron capture (Q_v = 2.79 MeV) renders the detector essentially insensitive, with the application of a suitable discriminator, to all other radiations. Knoll (Kn79) summarizes results with modified long counters that have achieved better uniformity and higher levels of sensitivity over more restricted energy domains.

9.5.3 Activation and Threshold Detectors

As we have seen, certain nuclear reactions have sharp thresholds which can be used to determine portions of a hadron spectrum that exceed it since the "leveling off" of the cross sections are generally well-behaved. In addition to information on reaction thresholds provided in Chapter 7, where referral was made to threshold techniques, Table 9.6 summarizes some of the useful reactions along with some pertinent information about threshold detectors that have been found to be useful in practical work. Some of these reactions will be discussed further below. Thomas and Stevenson (Th85 and Th88) provide a list of other reactions that might have useful thresholds.

Table 9.6 Important characteristics of various activation detector nuclear reactions

Detector	Reaction	Energy Range (MeV)	Half Life	Typical Detector Size	Cross Section-Peak (mb)	Cross Section-High Energy (mb)	Particle Detected
sulfur	$^{32}S(n,p)^{32}P$	> 3	14.3 d.	4 g disk	500[a]	10[a]	β^-
aluminum	$^{27}Al(n,\alpha)^{24}Na$	> 6	15 h	16 - 6600 g	11[b]	9[b]	γ
aluminum	$^{27}Al(n,x)^{22}Na$	> 25	2.6 y	17 g	30[b]	10[b]	γ
plastic scintillator	^{12}C - > ^{11}C	> 20	20.4 min	13-2700 g	90[b]	30[b]	β^+, γ
plastic scintillator	^{12}C -> ^{7}Be	> 30	53 d	17 g	18[b]	10[b]	γ
mercury	^{198}Hg - > ^{149}Tb	> 600	4.1 h	up to 500 g	2[b]	1[b]	α,γ
gold	^{197}Au -> ^{149}Tb	> 600	4.1 h	0.5 g	1.6[b]	0.7[b]	α,γ
copper	Cu -> ^{24}Na	> 600	14.7 h	580 g	4[c]	3.9[c]	γ
copper	Cu -> ^{52}Mn	> 70	5.7 d	580 g	5[c]	4.6[c]	γ
copper	Cu -> ^{54}Mn	> 80	310 d	580 g	11[c]	11[c]	γ

[a]Swanson and Thomas (Sw90)
[b]Barbier (Ba69)
[c]Baker, et al. (Ba84 and Ba91).

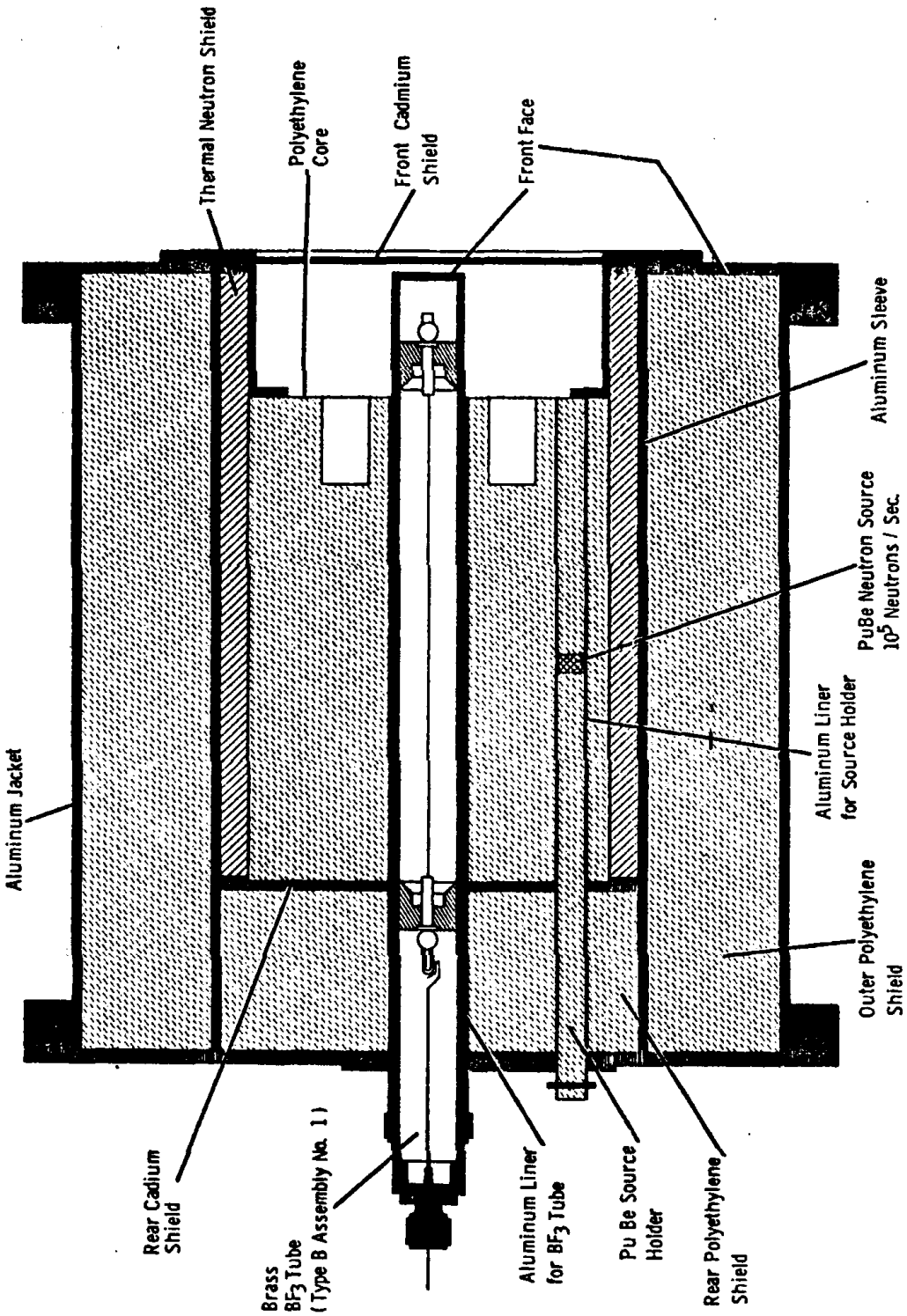

Fig. 9.10 Schematic diagram of a DePangher Long Counter. This version contained a built-in PuBe source, which is optional. The source would not be desirable in an instrument to be used in radiation fields near natural background. The dimensions and mass of this instrument are given in the text. [Reproduced from DeP66).]

The ^{12}C -> ^{11}C producing reactions are of special interest because of the fact that plastic scintillators can themselves become activated by hadrons (especially neutrons and protons) exceeding 20 MeV. This technique was first developed by McCaslin (McC60). The cross sections for this reaction, as initiated by several different types of incident particles, are shown in Fig. 9.11. Stevenson (St84b) has determined that a value of 28 fSv m^2 is an appropriate factor to apply to the conversion of the measured fluence of neutrons with E_n > 20 MeV to the dose equivalent due to those energetic neutrons. This assumes a typical accelerator spectrum found within thick shields of earth or concrete where neutrons clearly dominate. Such measurements can be useful to determine the contribution of the high energy (E_n > 20 MeV) neutrons to the total neutron dose equivalent.

Moritz (Mo89) has found that the use of NE102A scintillators activated by the $^{12}C(n, 2n)^{11}C$ can be included as an additional high energy detector in a Bonner sphere measurement in order to extend the energy range. Moritz, following Stevenson, used an average cross section of 22 mb for the $^{12}C(n,2n)^{11}C$ reaction. NE102A, a common and typical plastic scintillator, has a carbon content of 4.92 x 10^{22} atoms g^{-1} and a density of 1.032 g cm^{-3} according to Knoll (Kn79). Moritz used a cylindrical detector 5 cm in diameter by 5 cm long and achieved an efficiency of 93 % in detecting the 0.511 annihilation γ-rays produced as a result of the ^{11}C decay. In effect, the addition of this reaction reduced the degeneracy of the spectrum unfolding process using the code LOUHI.

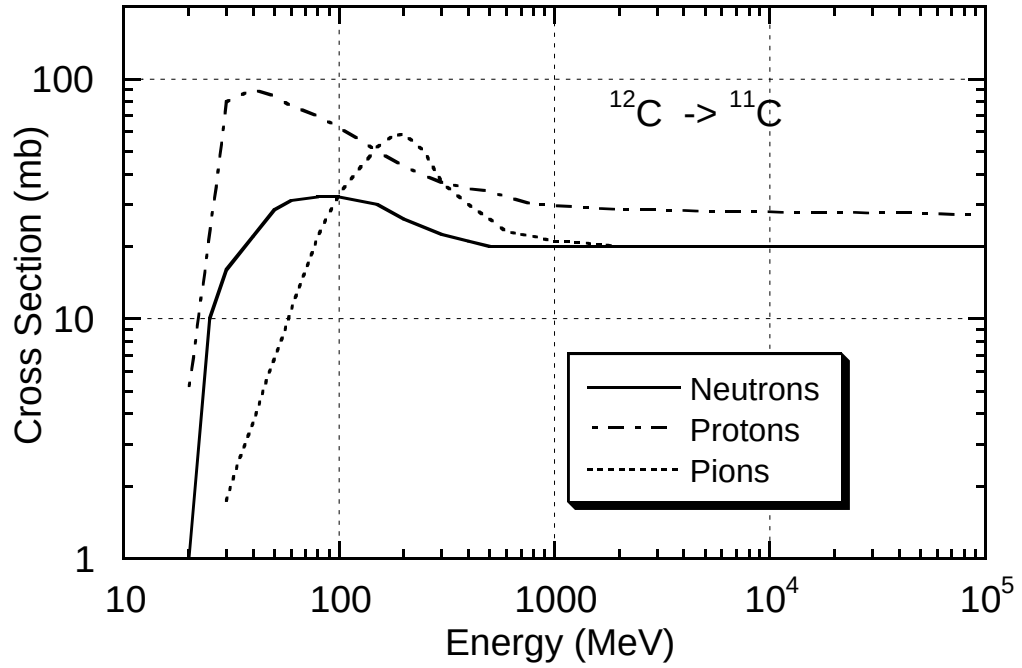

Fig. 9.11 Excitation functions for the reactions ^{12}C -> ^{11}C induced by neutrons, pions, and protons. The arithmetic mean of the positive and negative pions cross-sections is shown as the pion curve. [Adapted from (Sw90).]

Figure 9.12 provides the excitation functions of some other useful threshold reactions. The Hg -> ^{149}Tb reaction is a suitable monitor for very high energy particles and is commonly used as a beam calibrator. However, it has been found by Baker et al.(Ba84 and Ba91) that there are three reactions involving copper targets that are more useful for this purpose because they have longer half-lives than the 4.1-hr half life of ^{149}Tb. These cross sections have been measured for energies from 30 to 800 GeV and are included in Table 9.6.

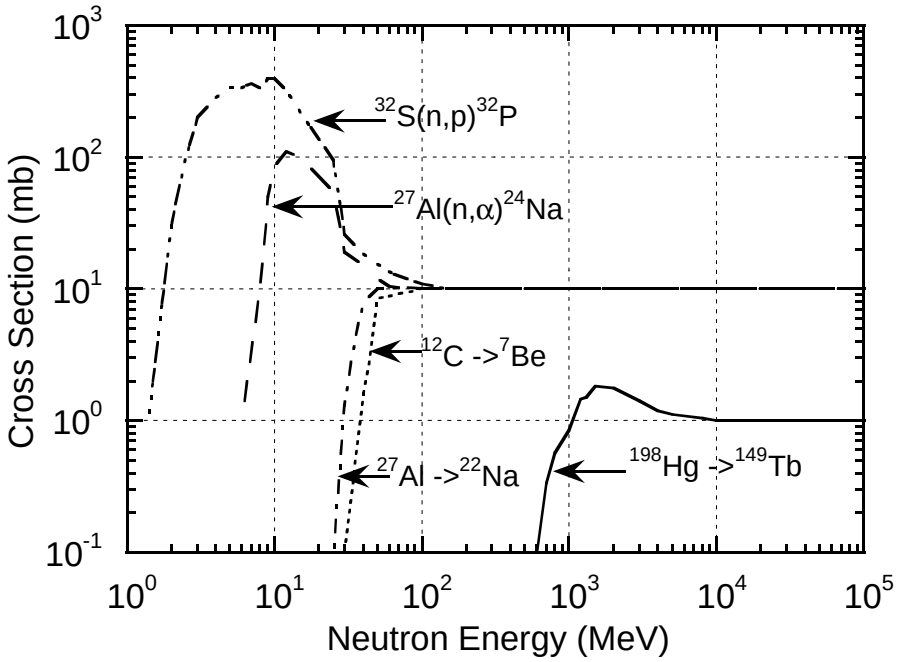

Fig. 9.12 Excitation functions of several threshold reactions. [Adapted from (Th88).]

9.5.4 Fission Counters

^{233}U, ^{235}U, and ^{239}Pu all have relatively large fission cross sections at low neutron energies. The *Q*-values are very large (approximately 200 MeV) so that huge output signals are possible. For higher energy "fast" neutrons, fission reactions become possible for other, lighter nuclei such as bismuth. The cross sections for fast neutrons of these reactions are shown in Fig. 9.13. Fission reactions have been exploited as neutron (or hadron) detectors at accelerators. The fission of ^{209}Bi is especially interesting since this reaction has a threshold of about 50 MeV and also exhibits strong evidence that the neutron and proton-induced fission cross sections are approximately equal. Bismuth has been employed in ionization chambers where the large energy deposited by the fission fragments gives a clear "signature" of this process. Like the use of ^{11}C, it can provide further information about high energy neutrons and resolve ambiguities in the unfolding of spectra from Bonner sphere data. McCaslin et.al. have summarized some interesting results obtained using this process (McC68).

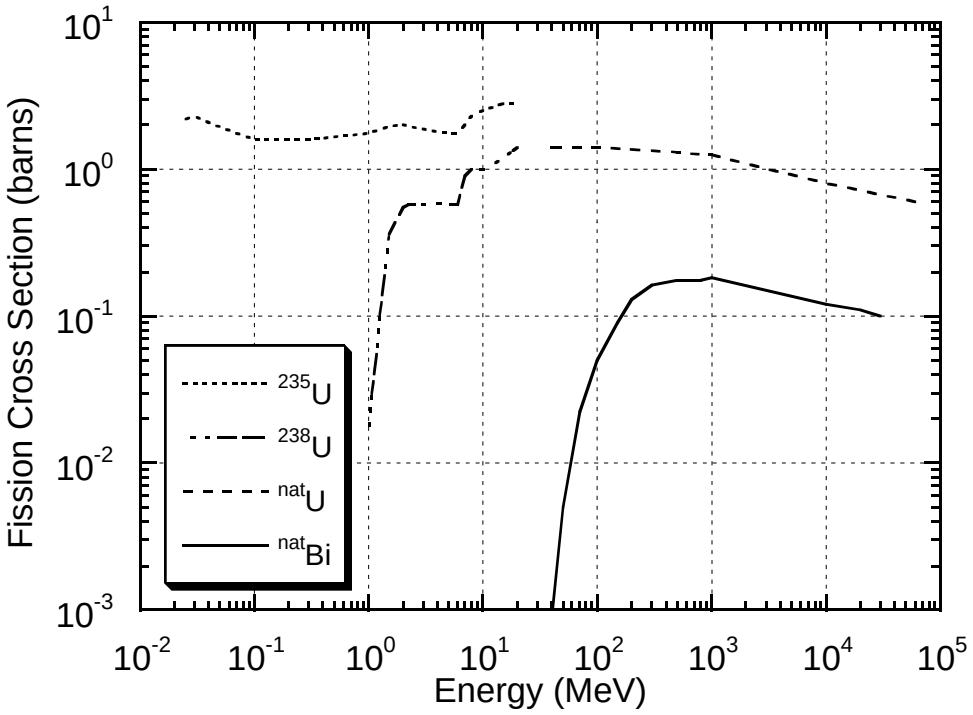

Fig. 9.13 Fission cross sections of some common target nuclides used in fission chambers for fast neutrons. The cross sections for fission at low energies for ^{235}U are much larger. [Adapted partially from (Kn79) and from (Sw90).]

9.5.5 Proton Recoil Counters

Knoll (Kn79) describes a variety of techniques for detecting neutrons based upon measuring the energy of recoil particles. The $^{3}He(n, p)^{3}H$ reaction has a reasonable cross section even into the MeV region but suffers from competition with (n, d) processes and elastic scattering. Elastic scattering of neutrons in which the energy of the recoil particle is measured and correlated with the neutron energy has received a great deal of attention. The most obvious recoil particle to measure is the proton because hydrogenous detector materials (e.g., plastic scintillator) are readily available and also because the proton can receive the most energy in the recoil process. Detector designers have been able to exploit the fact that scattering from hydrogen in the region $E_n < 10$ MeV is *isotropic* in the center of mass frame. Knoll has shown that the probability, $P(E_r)$, of creating a recoil with energy E_r is also independent of angle in the laboratory frame within this energy domain (Kn79). Thus the recoil energy is only a function of the incident neutron energy. However, complexities enter the picture because in scintillators, carbon is present along with the hydrogen and can contribute recoil protons. Furthermore, the magnitude of the cross sections is a function of neutron energy as is the efficiency of neutron detection in the scintillator. These effects, along with finite pulse height

resolution, can lead to the need to resort to unfolding techniques in which the pulse height, indicative of the energy of the recoil proton, is correlated with the average neutron energy which could produce such a pulse. The technique has exhibited some promise in measuring the energy spectra of neutron radiation fields. The best recent summary is that of Griffith and Thorngate (Gr85) who were able to determine neutron energy spectra in the region between 2 and 20 MeV.

9.5.6 TEPCs and LET Spectrometry

In mixed field dosimetry, a promising technique, now reaching commercial potential is that of the tissue-equivalent proportional chamber (TEPC) sometimes referred to as the "Rossi counter" after its inventor, H. Rossi (Ro55). The technique has been described by Brackenbush et al. (Br78). In this instrument, tissue equivalent walls are employed to apply the Bragg-Gray principle. In such chambers, the pressure is maintained at low values, only a few torr (a few hundred pascals) so that the energy deposited is kept small. Thus, the energy so deposited will be equal to the linear energy transfer of the particle multiplied by the path length. At these low pressures, the gas-filled cavity has the same emergy loss as does a sphere of tissue of diameter about 1 μm-hence an "equivalent diameter of 1 μm". In principle, determining the absorbed dose from events in such chambers is a straightforward unit conversion from a measured pulse height spectrum (calibrated in energy) to absorbed dose (in tissue) irrespective of the radiation field;

$$D(\text{rad}) = 1.602\times10^{-8}\,\frac{C}{\rho V}\sum_{h_1}^{h_2} hN(h)\,, \qquad (9.28)$$

where the summation is over channels corresponding to the radiation type of interest (see below), V is the sensitive volume (cm^3), ρ is the density ($g\ cm^{-3}$) and C converts the channel number to energy in MeV while h is the channel number and $N(h)$ is the number of counts in channel number h.

In such chambers, the transition between photon and neutron-induced events occurs at a pulse height of about 15 keV μm^{-1}. It is possible to determine the quality factor, Q, from a single TEPC measurement. Under the conditions stated above, one can unfold from the pulse height spectrum the distribution of absorbed dose as a function of LET, $D(L)$, using a formula derived by Rossi (Ro68). The formula is complicated by the fact that one must average over mean chord lengths in the chamber. Such a distribution is used to calculate quality factor, and hence the dose equivalent. The advent of microprocessors has now made such instruments feasible as portable instruments. Fig. 9.14 shows a typical pulse height spectrum for such an instrument. In higher energy fields, dose distributions due to other particles with the same characteristic shapes but larger pulse sizes appear as the ^2H,^3H, ^3He, ^4He and even ^7Li "drop points". This obviously will add complexities to the unfolding procedures in the determination of LET spectra. A more recent discussion of the application of this technique is given by Vasilik et al. (Va85).

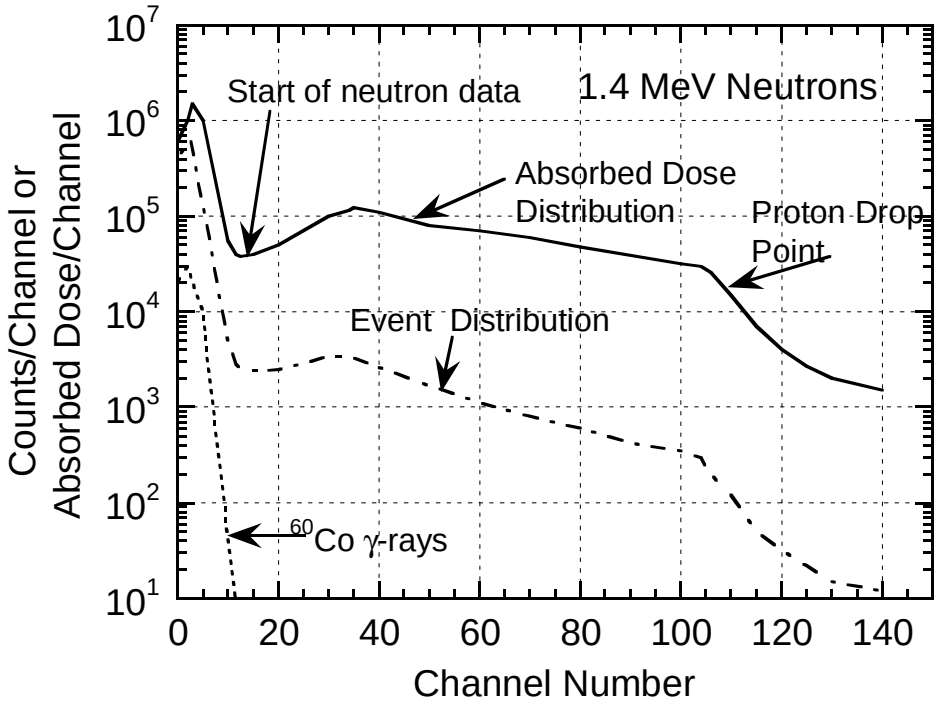

Fig. 9.14 Pulse-height spectra from a tissue-equivalent proportional counter exposed to 1.4 MeV neutrons and ^{60}Co γ-rays. [Adapted from (Br78).]

9.5.7 Recombination Chambers

An adaptation of the ion chamber that has shown considerable potential for usefulness as a dose equivalent meter in a mixed field of radiation is based on the exploitation of recombination phenomena in such chambers. As charged particles interact in such a chamber the gas is ionized. The electrodes will collect only those ions that do not recombine before they reach the cathode. Such **columnar recombination** will depend upon the average distance between the ions as well as upon the applied voltage. The biasing voltage sets the speed at which the ions migrate to the cathode. For a given voltage, a chamber should exhibit more severe recombination for the radiations having high LET (e.g. neutrons, heavy ions, etc.) than for those having low LET (electrons, photons, and muons). In the high LET situation, the slow moving positive ions are surrounded by a higher density of electrons than they would be in under conditions of low LET. Zielcyznski (Zi62) did the initial work on this topic. Later, Baarli and Sullivan (Ba65) reported similar results over a somewhat larger range of values of quality factor Q ($2 < Q < 20$).

Baarli and Sullivan further refined the technique (Ba65). It turns out that the current, i (or charge if integrated over time), measured in a given radiation field, is related to the applied voltage V by the following approximate expression:

$$i = kV^n. \tag{9.29}$$

The power, n, is approximately proportional to the quality factor Q and k is a constant proportional to the intensity of the radiation field. Cossairt et al. (Co84) have measured this effect using a mixed field of γ-rays and neutrons from a Pu-Be source. The results are shown in Fig. 9.15 over the range $1 \leq Q < 7$. The relationship between Q and n determined in (Co84) for one particular chamber was fit linearly by,

$$n = 0.00762 + 0.016Q, \tag{9.30a}$$

or by using a power law,

$$n = 0.019Q^{0.95}. \tag{9.30b}$$

Patterson and Thomas (Pa73) have reported similar results over a somewhat larger range of Q ($2 < Q < 20$). Typically, the response of such a chamber is measured as a function of applied voltage for the special chamber provided for the purpose over the voltage range $20 \leq V \leq 1200$ volts. In fields that are not steady with time, the response typically needs

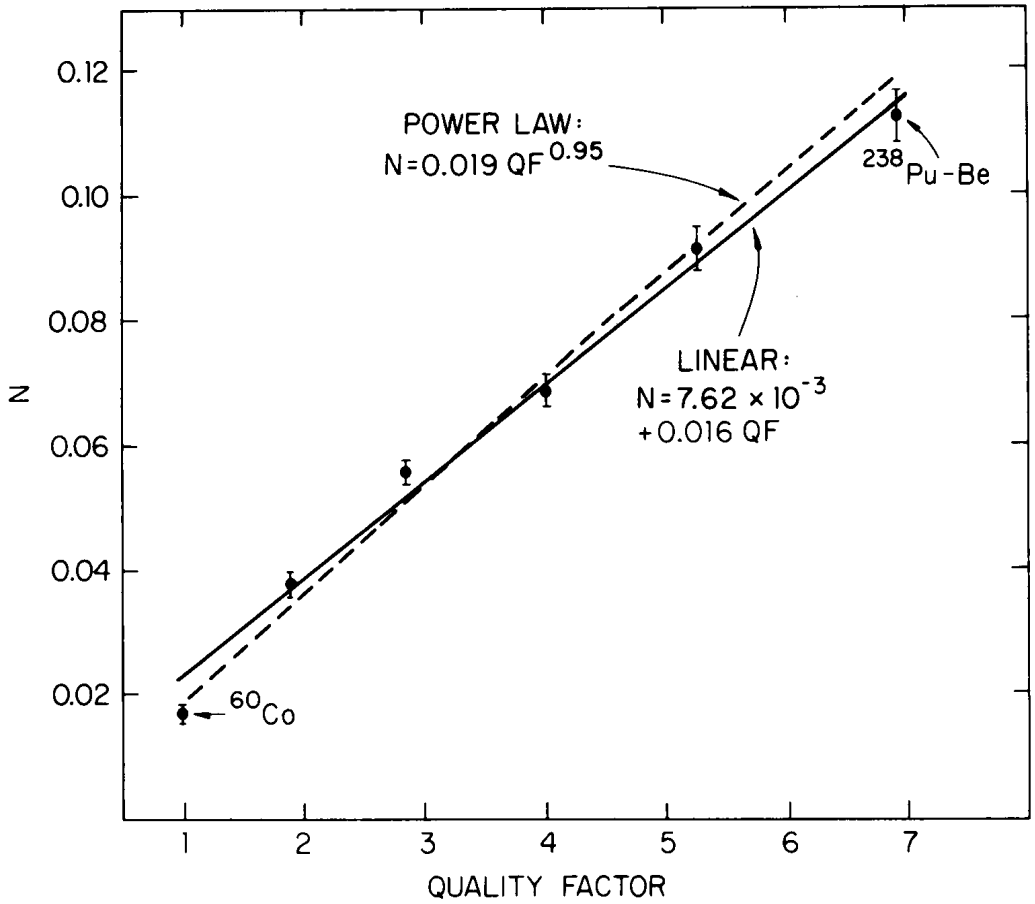

Fig. 9.15 Response of a recombination chamber as a function of quality factor Q obtained in mixed fields using radioactive sources. Two different fits to the data are presented [Reproduced from (Co84 and Co85b).]

to be normalized against some instrument that accurately measures the intensity of the radiation field. The method of least squares is then applied to determine *n* by taking advantage of the fact that Eq. (9.29) can be rewritten as

$$\ln i = \ln k + n \ln V \,. \tag{9.31}$$

In typical measurement, such a log-log fit to the data is of moderately good quality. The quality factor, *Q*, then, can be determined directly from *n* using a version of Eq. (6.30) determined for the particular recombination chamber used. Fig. 9.16 shows the response measured in a field known to be dominated by muons ($Q = 1$). Data taken in the iron leakage spectrum described in connection with Fig. 6.8 are shown in Fig. 9.17. Measurements of this type have been used to check the quality factors obtained in the unfolding of Bonner sphere data. Table 9.7 illustrates the typical agreement between these entirely different techniques for diverse radiation fields.

Zel'chinskij and Zharnovetskij (Ze67) proposed using two chambers placed in the radiation field of interest; one operated at a low voltage and other at a high voltage. The differences in responses read out by the two chambers would then be proportional to the dose equivalent rate. It turns out that measuring differences in ion chamber currents found in practical chambers is difficult due to the small currents and electrical leakage problems at the cable connectors.

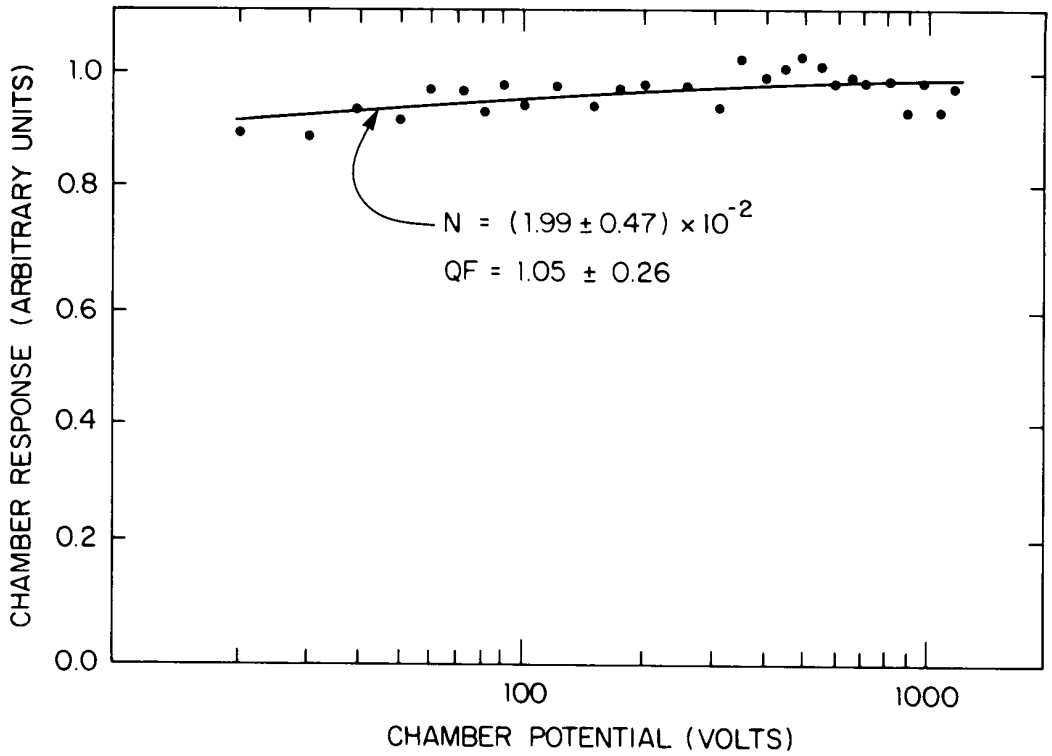

Fig. 9.16 Recombination chamber response as a function of chamber potential in a radiation field nearly completely consisting of high energy muons. [Reproduced from (Co87).]

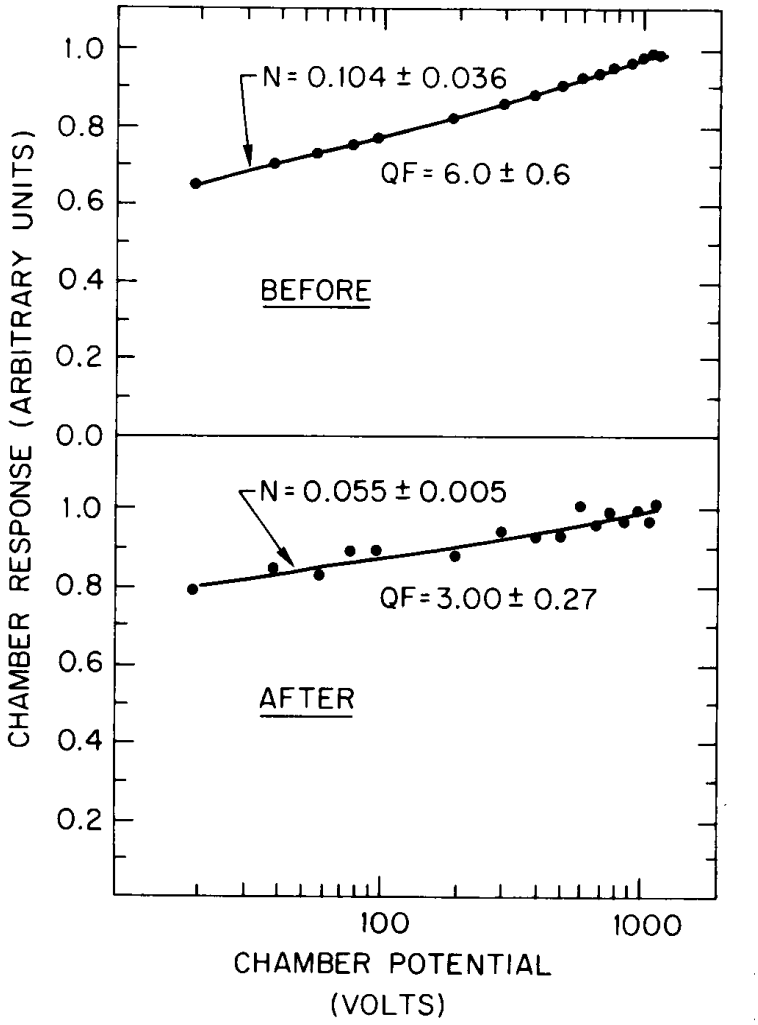

Fig. 9.17 Recombination chamber response functions measured both before (**top**) and after (**bottom**) the placement of additional shielding in the radiation field described in Fig. 6.8. [Reproduced from (El86).]

Table 9.7 Average quality factors obtained for various neutron energy spectra measurements at Fermilab. [Adapted from (Co88).]

Description of Radiation Field	**Technique**	
	Unfolding	**Recombination**
Mixed field of neutrons and muons (Co 87)	1.4 ± 0.2	1.1 ± 0.3
Iron leakage spectra before shielding was added (Fig. 6.8b) (El86)	5.4 ± 0.2	6.0 ± 0.6
Iron leakage spectra after shielding was added (Fig. 6.8c) (El86)	2.5 ± 0.3	3.0 ± 0.3
Spectrum in a labyrinth (Fig. 6.7) (Co85b)	3.1 ± 0.7	3.4 ±0.1

Höfert and Raffnsøe (Hö80) have measured the dose equivalent response of such an instrument as a function of neutron energy and obtained the results in Table 9.8.

Table 9.8 Dose equivalent response and measurement errors for recombination chamber as a function of neutron energy [Adapted from (Hö80).]

Neutron Energy (MeV)	Dose Equivalent Response (10^5 Coulombs Sv^{-1})	Error (%)
thermal	0.830	10.0
0.0245	2.579	12.1
0.1	1.451	6.2
0.25	1.585	6.1
0.57	1.215	5.2
1.0	1.215	5.2
2.5	1.112	6.1
5.0	0.840	5.2
15.5	0.728	5.2
19.0	0.998	12.1
280.0	0.782	10.1

9.5.8 Counter Telescopes

Since the dose equivalent per fluence for muons varies so little over a wide range (see Fig. 1.4), scintillation telescopes provide an attractive method for assessing pure muon fields. At suitable distances and at forward angles, muons will dominate the radiation fields and the result is that little or no discrimination against other particles is necessary.

At Fermilab, a pair of 20.32 cm square by 0.635 cm thick plastic scintillators has been used routinely (Co83). The separation distance between theses "paddles" provides moderate directional sensitivity when a coincidence is required between the two scintillator paddles in a relatively parallel beam of muons. An aluminum plate, 2.54 cm thick, is employed in the gap between the two scintillators to reduce false coincidences due to recoil electrons (so-called "δ-rays") produced in collisions occurring in the first scintillator that might reach the second if the aluminum were absent. These plates are mounted in an all-terrain vehicle, called the Mobile Environmental Radiation Laboratory (MERL), and are supported by an on-board electrical generator. A microwave telemetry system provides gating pulses and proton beam intensity information so that normalized beam-on and beam-off (background) measurements can be taken simultaneously. The paddles were chosen to provide sufficient sensitivity to obtain statistical errors at the 20 % level in remote locations receiving annual dose equivalents in the fractional mrem range in a scan lasting an hour or two. In such a scan, the detectors are moved across a region of elevated muon flux density. In these detectors, a muon beam perpendicular to the detectors yields 1.7×10^5 counts per minute per mrem/hour (or 1.02×10^7 counts $mrem^{-1}$). The normal singles background due to cosmic rays is approximately 400 counts per minute.

Smaller, more portable systems can be useful in conducting muon surveys. Fermilab has

built such a system, called a **muon finder**, consisting of a pair of small plastic scintillators mounted in a compact package which is battery powered and can be carried by one person. It is read out by scalers and can record both singles and coincidence rates. The ratio of the two can be used to "find" unknown muon sources; hence the name of the detector. Also, the separation distance can be adjusted to enhance, or reduce, the directional sensitivity.

The parameters of this system are given in Table 9.9. Of course, the use of such scintillators, especially in the "singles" mode, in mixed fields of muons and neutrons requires that one must be aware of the fact that the plastic scintillators have nonzero detection efficiency for the neutrons. Vylet has used the values of total cross sections to calculate the neutron detection efficiency of the detectors described above for neutrons over a range of energies (Vy91). The results are given in Fig. 9.18. In this figure, effects due to successive collisions as well as those due to the first collisions with hydrogen atoms ("1st collision with H") are given. The total efficiencies at the upper end of the energy region measured were an efficiency of 0.058 for the MERL paddles and 0.0235 for the muon finders.

Table 9.9 Parameters of the "muon finder" used at Fermilab

Scintillator diameter	2.1 cm
Scintillator thickness	0.635 cm
Scintillator area	3.6 cm^2
Scintillator spacing	0.5 to 8.9 cm
Half-angle cone of sensitivity	0.9 to 0.2 radians (51 to 11.5 deg. half-angle)
Dose equivalent calibration (muons $\perp$ detectors)	90 muons/μrem
Dose equivalent rate calibration (muons $\perp$ detectors)	25 muons/sec per mrem/hour

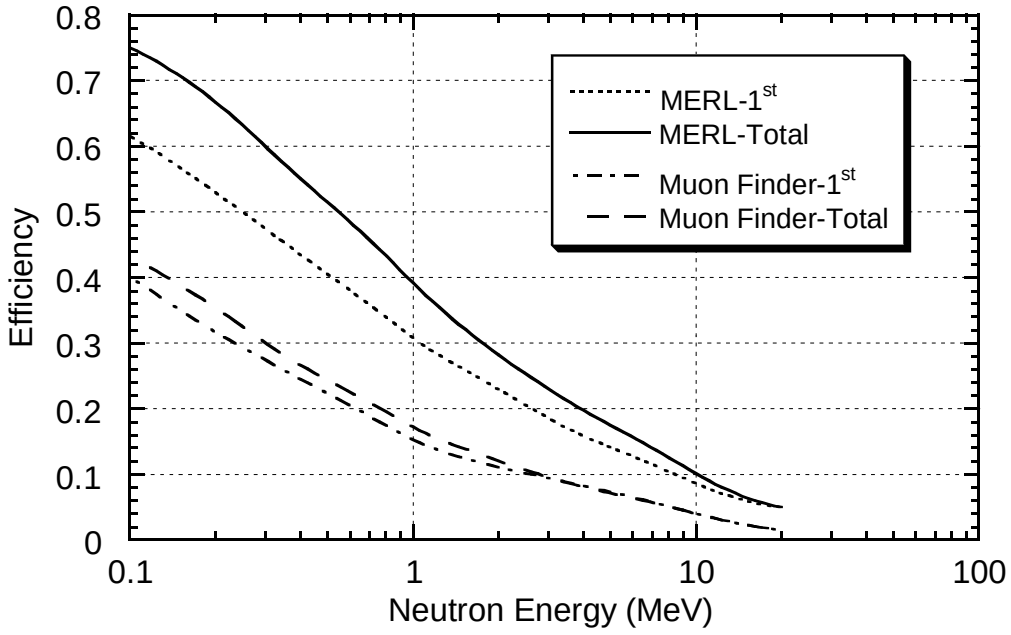

Fig. 9.18 Calculated neutron efficiencies of scintillation counters used in the "singles" mode at Fermilab as a function of neutron energy as described in the text. [Adapted from (Vy91).]

Problems

1. A cylindrical ion chamber is 5 cm in radius and 20 cm long. It is filled with methane (CH_4) at 1 one atmosphere absolute pressure. It is bombarded by a uniform flux density of high energy (minimum-ionizing) muons incident perpendicularly to one of the ends. One can safely make the assumption that the passage of the muons through the entire length of the chamber represents insignificant degradation of the muon energy or direction. The dose equivalent rate in the radiation field is 0.1 mrem $hour^{-1}$.

   a) Calculate the electric current that will be drawn from this chamber that represents the "signal" to be measured and correlated with the dose equivalent rate. One needs to use Table 1.2 to obtain values of $(dE/dx)_{min}$ and to obtain the density of CH_4.

   b) If the charge liberated in the chamber is collected (i.e., integrated electronically) for 1 second and the chamber and circuit represent a capacitance of 10^{-10} Farads, calculate the size of the signal pulse in volts if one neglects any "pulse-shaping" of the readout electronics.

2. Consider the detector based on the 25.4 cm moderating sphere for which the corresponding response curve is displayed in Fig. 9.8.

   a) Calculate the approximate absolute intrinsic detection efficiency for neutrons. This is to be done for the $2 < E_n < 8$ MeV energy domain and the sharp peaks in the detector response curve are to be ignored (i.e., averaged out). In this problem, 100 % efficiency is defined to be 1 count generated for every neutron that strikes the sphere. Assume the incident neutrons to be monodirectionally aimed at the detector and originate from a "point" source" despite the fact that this is not quite true.

   b) Since the LiI detector only responds to thermal neutrons, calculate the efficiency with which the moderator transforms fast neutrons incident upon it into thermal neutrons present at the LiI. For this calculation, neglect any "dopants" in the LiI, assume that the Li is "natural" lithium with respect to isotopic abundance and use the fact that the atomic weight of iodine is 127. The density of LiI is 3.5 g cm^{-3}. Assume that the detector is 100% efficient in detecting thermal neutron captures within its volume.

3. A BF_3 proportional chamber is used in a DePangher long counter. This detector, when placed in a certain neutron field that is known to be dominated by neutrons of approximately 5 MeV kinetic energy, generates counts due to neutrons at the rate of 1 count/minute. The detector sensitivity is that discussed in the text. The counter operates at one atmosphere absolute pressure, the atomic weight of boron is 10.8 while the atomic weight of fluorine is 19. At STP the density of BF_3 is 2.99 grams liter^{-1}.

   a) What is the dose equivalent rate of this radiation field?

   b) If the radiation field persists full time, is this detector sufficiently sensitive to detect a dose rate of 10 mrem year^{-1}?

   c) In this radiation field, high energy minimum ionizing muons pass through this detector, including the proportional counter. The largest muon signals in the proportional counter will obviously result when the muons pass lengthwise through the tube. If the tube is 40 cm long, what will be the size of the largest muon-induced signal relative to the neutron-induced signal? Is it likely that a simple discriminator circuit can be used to eliminate the muon-induced signals? It is quite permissible to estimate the value of $(dE/dx)_{min}$ by roughly interpolating among the values tabulated in Table 1.2.

4. One needs to understand the sensitivity of the technique of using the $^{12}C(n, 2n)^{11}C$ reaction in plastic scintillator to measure dose equivalent rate external to thick concrete or earth shielding near a high energy accelerator. The detector discussed in the text used by Moritz has a sensitive volume of approximately 100 cm^3 (a 5 cm diameter by 5 cm long cylinder). The NE102A scintillator, from Knoll (Kn79), has a density of 1.032 g cm^{-3}. This detector is nearly 100 % efficient at sensing the 0.511 MeV annihilation photons produced in the course of the ^{11}C decay.

   a) This detector is irradiated in a particular radiation field external to such accelerator shielding. The irradiation, which is steady in time, is of sufficient length in time to result in saturation of the production of ^{11}C in the scintillator. After the beam is turned off, the detector counts at a rate of 10 counts per minute (including appropriate decay-correction to the instant of beam shutdown). Calculate the flux density of neutrons with E_n > 20 MeV during the irradiation and use the result along with Stevenson's conclusion concerning the conversion from the flux density of neutrons with E_n > 20 MeV to dose equivalent to determine the dose equivalent rate.

   b) Assuming this count rate is the smallest that can be reliably detected, how much smaller in volume can the detector be for it to barely be sensitive to a dose equivalent rate of 2 mrem hour^{-1}?